

## REPORT 1014

### STUDY OF EFFECTS OF SWEEP ON THE FLUTTER OF CANTILEVER WINGS<sup>1</sup>

By J. G. BARMBY, H. J. CUNNINGHAM, and I. E. GARRICK

#### SUMMARY

*An experimental and analytical investigation of the flutter of sweptback cantilever wings is reported. The experiments employed groups of wings swept back by rotating and by shearing. The angle of sweep ranged from 0° to 60° and Mach numbers extended to approximately 0.85. A theoretical analysis of the air forces on an oscillating swept wing of high length-chord ratio is developed, and the approximations inherent in the assumptions are discussed. Comparison with experiment indicates that the analysis developed in the present report is satisfactory for giving the main effects of sweep, at least for nearly uniform cantilever wings of high and moderate length-chord ratios. A separation of the effects of finite span and compressibility in their relation to sweep has not been made experimentally but some combined effects are given. A discussion of some of the experimental and theoretical trends is given with the aid of several tables and figures.*

#### INTRODUCTION

The present report is an outgrowth of the trend toward the use of swept wings for high-speed flight and presents the results of an analysis and of an accompanying exploratory program of research in the Langley 4.5-foot flutter research tunnel on swept cantilever wings. The material was assembled in a memorandum form with a similar title in 1948. The chief purposes of the present report are to provide a more detailed exposition of the analysis and to make the main material more generally available.

Some previous experimental and analytical work on swept wings is mentioned here. A preliminary experimental investigation of the effect of sweep on flutter has been made (reference 1) with a single, simple rigid wing mounted flexibly on a base which could be rotated to various desired sweep angles. This investigation was made at low Mach numbers for two bending-torsion frequency ratios and at several angles of sweepback. Another investigation (data unpublished) in which the density of the test medium was a variable was conducted by D. Benun on the same type of rigid, flexibly mounted wing at higher Mach numbers and at sweep angles of 0° and 45°. Other unpublished work on swept wings exists, but a search of the available information indicates a need for further systematic study.

The experimental work reported herein dealt with models mounted as cantilevers at their roots. These cantilever models differed from the rigid, flexibly mounted wings, which had all bending and torsion flexibility concentrated at the root, and thus were subject to different root effects. In order to facilitate analysis the cantilever models were uniform and untapered. The intent of the experimental program was to establish trends and to indicate orders of magnitude of the various effects of sweep on flutter rather than to isolate precisely the separate effects.

The models were swept back in two basic manners—shearing and rotating. For the case in which the wings were swept back by shearing the cross sections parallel to the air stream, the span and aspect ratio remained constant. For the other case, a series of rectangular-plan-form wings were mounted on a special base which could be rotated to provide any desired angle of sweepback. This rotatory base was also used to examine the critical speed of swept-forward wings.

Tests were conducted also on special models that were of the "rotated" type (sections normal to the leading edge were the same at all sweep angles) with the difference that the bases were aligned parallel to the air stream. Two series of such rotated models having different lengths were tested.

Inasmuch as the location of the center of gravity, the mass-density ratio, and the Mach number have important effects on the flutter characteristics of unswept wings, these parameters were varied for swept wings. In order to investigate possible changes in flutter characteristics which might be due to different flow over the tips, various tip shapes were included in the experiments.

In an analysis of flutter, vibrational characteristics are very significant; accordingly, vibration tests were made on each model. A special study of the change in frequency and mode shape with angle of sweep was made for a simple aluminum-alloy beam and is reported in appendix A.

Theoretical analyses of the effect of sweep on flutter exist only in brief or preliminary forms. In England in 1942, W. J. Duncan estimated by certain dimensional considerations the effect of sweep on the flutter speed of certain specialized wing types. Among other British workers whose names are mentioned in connection with problems

<sup>1</sup> Supersedes NACA TN 2121, "Study of Effects of Sweep on the Flutter of Cantilever Wings" by J. G. Barmby, H. J. Cunningham, and I. E. Garrick, 1950.

of flutter involving sweep are R. McKinnon Wood, A. R. Collar, and I. T. Minhinick. An account of Minhinick's work was given by Broadbent in reference 2. In reference 3 a preliminary analysis for the flutter of swept wings in incompressible flow is developed on the basis of a "strip theory" (with the strips taken in the stream direction) and is applied to the experimental results of reference 1. Examination of the limiting case of infinite span discloses that the aerodynamic assumptions employed in reference 3 are not well-grounded. Reference 4 adapts this strip theory to flexible wings and also presents an alternative "velocity component" treatment employing other aerodynamic assumptions which in their end result appear more akin to those employed in the analysis of the present report. No definite choice is made in reference 4 between the two methods although the strip-theory method is favored.

In the present report a theoretical analysis is developed anew and given a general presentation. Application of the analysis has been limited at this time chiefly to those calculations needed for comparison with experimental results. A wider examination of the effect of various parameters and of additional degrees of freedom on the flutter characteristics is desirable.

## SYMBOLS

$b$	half-chord of wing measured perpendicular to elastic axis, feet
$b_r$	half-chord perpendicular to elastic axis at reference station, feet
$l'$	effective length of wing, measured along elastic axis, feet
$c$	wing chord measured perpendicular to elastic axis, inches
$l$	length of wing measured along midchord line, inches
$\Lambda$	angle of sweep, positive for sweepback, degrees
$A_s$	geometric aspect ratio $\left(\frac{l \cos \Lambda}{lc}\right)$
$x'$	coordinate perpendicular to elastic axis in plane of wing, feet
$y'$	coordinate along elastic axis, feet
$z'$	coordinate in direction perpendicular to $x'y'$ -plane, feet
$Z$	coordinate of wing surface in $z'$ -direction, feet
$\eta$	nondimensional coordinate along elastic axis ( $y'/l'$ )
$\xi$	coordinate in wind-stream direction
$h$	bending deflection of elastic axis, positive downward, feet
$\theta$	torsional deflection of elastic axis, positive with leading edge up, radians
$\sigma$	local bending slope of elastic axis $\left(\frac{\partial h}{\partial y'}\right)$
$\tau$	local rate of change of twist $\left(\frac{\partial \theta}{\partial y'}\right)$
$f_h(y'), F_h(\eta)$	deflection function of wing in bending
$f_\theta(y'), F_\theta(\eta)$	deflection function of wing in torsion
$t$	time
$\omega$	angular frequency of vibration, radians per second

$\omega_h$	angular uncoupled bending frequency, radians per second
$\omega_\alpha$	angular uncoupled torsional frequency about elastic axis, radians per second
$f_{h_1}$	first bending natural frequency, cycles per second
$f_{h_2}$	second bending natural frequency, cycles per second
$f_t$	first torsion natural frequency, cycles per second
$f_\alpha$	uncoupled first torsion frequency relative to elastic axis, cycles per second $\left(f_t \left[1 - \frac{(x_a/r_a)^2}{1 - (f_{h_1}/f_t)^2}\right]^{\frac{1}{2}}\right)$
$f_e$	experimental flutter frequency, cycles per second
$f_R$	reference flutter frequency, cycles per second
$f_A$	flutter frequency determined by analysis of present report, cycles per second
$v$	free-stream velocity, feet per second
$v_e$	experimental flutter speed, feet per second
$v_n$	component of air-stream velocity perpendicular to elastic axis, feet per second ( $v \cos \Lambda$ )
$V_e$	experimental flutter speed taken parallel to air stream, miles per hour
$V_R$	reference flutter speed, miles per hour
$V_R'$	reference flutter speed based on wing elastic axis, miles per hour (defined in appendix B)
$V_A$	flutter speed determined by theory of present report, miles per hour
$V_D$	theoretical divergence speed, miles per hour
$k_n$	reduced frequency employing velocity component perpendicular to elastic axis ( $\omega b/v_n$ )
$\varphi$	phase difference between wing bending and wing torsion strains, degrees
$\rho$	density of testing medium at flutter, slugs per cubic foot
$q$	dynamic pressure at flutter, pounds per square foot
$M$	Mach number at flutter
$M_{cr}$	critical Mach number
$x_{cg}$	distance of center of gravity behind leading edge taken perpendicular to elastic axis, percent chord
$x_{ea}$	distance of elastic center of wing cross section behind leading edge taken perpendicular to elastic axis, percent chord
$x_{ea}'$	distance of elastic axis of wing behind leading edge taken perpendicular to elastic axis, percent chord
$a$	nondimensional elastic-axis position $\left(\frac{2x_{ea}}{100} - 1\right)$
$a + x_\alpha$	nondimensional center-of-gravity position $\left(\frac{2x_{cg}}{100} - 1\right)$
$m$	mass of wing per unit length, slugs per foot
$\kappa$	wing mass-density ratio at flutter ( $\pi \rho b^2/m$ )
$I_\alpha$	mass moment of inertia of wing per unit length about elastic axis, slug-feet <sup>2</sup> per foot

$r_\alpha$	nondimensional radius of gyration of wing about elastic axis ( $\sqrt{\frac{I_\alpha}{mb^2}}$ )
$EI$	bending stiffness, pound-inches <sup>2</sup> in tables, pound-feet <sup>2</sup> in analysis
$GJ$	torsional stiffness, pound-inches <sup>2</sup> in tables, pound-feet <sup>2</sup> in analysis
$g_h$	structural damping coefficient for bending vibration
$g_\alpha$	structural damping coefficient for torsional vibration
$P$	oscillatory lift per unit length, positive downward (defined in equation (6))
$M_\alpha$	oscillatory moment about elastic axis, positive leading edge up (defined in equation (7))
[ ]	a special bracket used to identify terms which are due solely to inclusion of the last term in equation (5b)

In order to preserve continuity and to facilitate comparison with previous work on the unswept wing, the subscript  $\alpha$  rather than  $\theta$  is retained with certain quantities to refer to the torsional degree of freedom.

## ANALYTICAL INVESTIGATION

### GENERAL

**Assumptions.**—An attempt is first made to point out the main assumptions which seem to be applicable for swept wings of moderate taper and of high or moderate length-chord ratios.

(a) The assumptions, such as small disturbances and potential flow, commonly employed in linearized treatment of unswept wings in an ideal incompressible fluid are made.

(b) The structural behavior is such that over the main part of the wing the elastic axis may be considered straight. The wing is also considered sufficiently stiff at the root so that it behaves as if it were clamped normal to the elastic axis. An effective length  $l'$  needed for integration reasons may be defined (for example, as in fig. 1). The angle of sweepback is measured in the plane of the wing from the direction normal to the air stream to the elastic axis. All section parameters such as semichord, locations of elastic axis and center of gravity, radius of gyration, and so forth, are based on sections normal to the elastic axis.

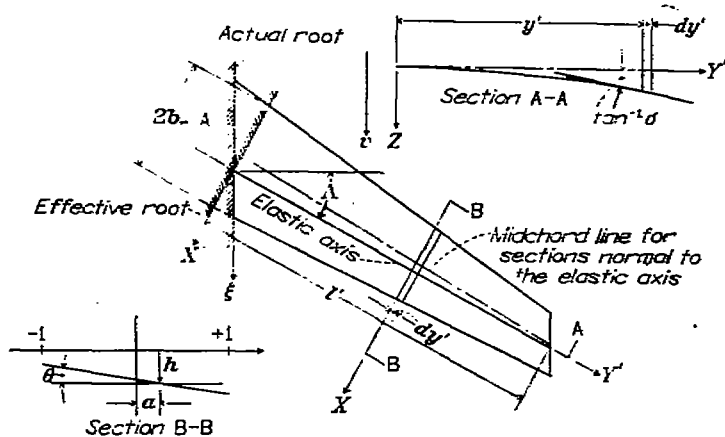


FIGURE 1.—Nonuniform swept wing treated in the present analysis.

(c) The aerodynamic behavior is such that any section  $dy'$  of the wing normal to the elastic axis, taken in the direction of the component  $v \cos \Lambda$  of the main-stream velocity, generates a velocity potential associated with a uniform infinite swept wing having the same instantaneous distribution over the chord of velocity normal to the wing surface as does the actual section.

Additional remarks on these assumptions are appropriate. With regard to assumption (a), in accordance with linearization of the problem, the boundary conditions are stated and treated with respect to a reference surface, in this case a plane, containing the mean equilibrium position of the wing and the main-stream velocity. Furthermore, incompressible flow is assumed in order to avoid complexity of the analysis, although modifications due to Mach number effects can be added. Such modifications may be based, for example, for wings having large length-chord ratios, on existing theoretical calculations of aerodynamic coefficients for subsonic or supersonic two-dimensional flow appropriate to the component  $v \cos \Lambda$ . On the other hand the modifications may be partly empirical, especially for "transonic" conditions and for small length-chord ratios. The transonic conditions and the general aerodynamic behavior of swept wings may depend, for large length chord ratios, on the component  $v \cos \Lambda$ , but the dependence may shift to the stream velocity  $v$  for small length-chord ratios.

With respect to assumption (b), results of analyses of and experiment on unswept wings having low ratios of bending frequency to torsion frequency show that small variations of position of the elastic axis are not important. The assumption of a straight elastic axis over the main part of a swept wing, similarly, is not critical for many cases. This assumption is made for convenience, however, and modifications for a curved elastic axis can be made when necessary, for example, for plate-like wings. Small differences in the angle of sweepback of the leading edge, quarter-chord line, elastic axis, and so forth, are neglected. The analysis could be further modified to take into account variation of the angle of sweepback along the length of the wing.

Assumption (c) implies that associated with the action of the wing in pushing air downward there is a noncirculatory potential-type flow similar to that around sections of an infinite flat-plate wing. Furthermore, as in the case of the unswept airfoil, a circulatory potential-type flow is generated in which for the swept airfoil the component  $v \cos \Lambda$  is decisive in fixing the circulation. (This assumption differs from that made in the strip theory of references 3 and 4 which employs the main-stream velocity together with sections of the wings parallel to the stream direction.) Effects of the floating of the wake in the stream direction rather than in the direction of  $v \cos \Lambda$  and induced effects of variation of the strength of the wake in the wing-length direction are neglected, as are three-dimensional tip effects. For large values of the reduced frequency  $k_\alpha$ , a given segment of the wing might be influenced chiefly by the nearby wake and the correction would be small. On the other hand, for small values of  $k_\alpha$ , a given segment might be influenced by a more widespread portion of the wake; corrections for this condition may possibly be based on knowledge of the static

case (for example, slope of the lift curve). As the angle of sweep approaches  $90^\circ$ , obviously the mechanism for the generation of lift is different from the one postulated here; for example, a tip condition may replace the trailing-edge condition and considerations of very small aspect ratio arise.

**Basic considerations.**—Consider the configuration shown in figure 1 where the vertical coordinate of the wing surface is denoted by  $z' = Z(x', y', t)$  (positive downward). The effect of the position and motion of the wing may be given by the disturbance-velocity distribution to be superposed on the uniform stream in order to represent the condition of tangential flow at the wing surface. This velocity distribution normal to the surface (positive upward) is, for small disturbances,

$$w(x', y', t) = \frac{\partial Z}{\partial t} + v \frac{\partial Z}{\partial \xi} \quad (1a)$$

where  $\xi$  is the coordinate in the wind-stream direction. With the use of the relation

$$\begin{aligned} \frac{\partial Z}{\partial \xi} &= \frac{\partial Z}{\partial x'} \frac{\partial x'}{\partial \xi} + \frac{\partial Z}{\partial y'} \frac{\partial y'}{\partial \xi} \\ &= \frac{\partial Z}{\partial x'} \cos \Lambda + \frac{\partial Z}{\partial y'} \sin \Lambda \end{aligned}$$

the vertical velocity at any point is

$$w(x', y', t) = \frac{\partial Z}{\partial t} + v \frac{\partial Z}{\partial x'} \cos \Lambda + v \frac{\partial Z}{\partial y'} \sin \Lambda \quad (1b)$$

Let the wing be bending so that a segment  $dy'$  (see fig. 1) is displaced from its equilibrium position by an incremental distance  $h$  (positive down) and also let the wing segment be twisting about the elastic axis through an incremental angle  $\theta$  (positive leading edge up). The position of each point of the segment may be defined, for small deflections, by

$$Z = h + x' \theta \quad (2)$$

The velocity distribution normal to the surface, equation (1b), consequently becomes

$$w = \dot{h} + x' \dot{\theta} + v \theta \cos \Lambda + v(\sigma + x' \tau) \sin \Lambda \quad (3)$$

where  $\sigma = \frac{\partial h}{\partial y'}$  is the local bending slope of the elastic axis and is thus analogous to dihedral, and where  $\tau = \frac{\partial \theta}{\partial y'}$  is the local change of twist of the elastic axis.

In accordance with assumption (c) the noncirculatory-flow velocity potentials associated with the vertical-velocity distribution are first needed. In equation (3) the terms involving  $\dot{h}$ ,  $\dot{\theta}$ , and  $\sigma$  are constant across the chord, whereas those

involving  $\theta$  and  $\tau$  vary in a linear manner. The noncirculatory velocity potentials as in reference 5 and the new potentials associated with  $\sigma$  and  $\tau$  are

$$\left. \begin{aligned} \phi_h &= \dot{h} b \sqrt{1-x^2} \\ \phi_\theta &= v_\infty \theta b \sqrt{1-x^2} \\ \phi_\sigma &= v_\infty \sigma \tan \Lambda b \sqrt{1-x^2} \\ \phi_i &= \theta b^2 \left( \frac{x}{2} - a \right) \sqrt{1-x^2} \\ \phi_\tau &= v_\infty \tau \tan \Lambda b^2 \left( \frac{x}{2} - a \right) \sqrt{1-x^2} \end{aligned} \right\} \quad (4)$$

where  $v_\infty = v \cos \Lambda$  and  $x$  is the nondimensional chordwise coordinate measured from the midchord as in reference 5 and related to the coordinate  $x'$  in the manner

$$x = \frac{x'}{b} + a$$

The velocity potential for the circulatory flow associated with the wake may be developed on the basis of assumption (c) and the concepts for the infinite unswept wing introduced in reference 5. (Thus the circulatory-flow pattern for a section  $dy'$  of the finite swept wing is to be obtained from the corresponding flow pattern for an infinite uniform yawed wing. This infinite wing is assumed to have undergone harmonic oscillations for a long time; the full wake is established, remains where formed, and consequently is harmonically distributed in space. For the infinite uniform yawed wing, results for the circulatory flow are like those of reference 5 with  $v$  replaced by the component  $v_\infty$  and with the addition of terms to take care of  $\sigma$  and  $\tau$ .) In particular, the strength of the wake acting on each section is determined by the condition of smooth flow (the velocity remaining finite) at the trailing edge. This condition is utilized in the form  $\frac{\partial}{\partial x} (\phi_r + \phi_N)$  is equal to a finite quantity at the trailing edge (where  $\phi_r$  is the velocity potential due to the vorticity in the wake, and  $\phi_N$  is the total noncirculatory velocity potential), and this condition leads to a relation analogous to equation (VII) of reference 5 involving the basic quantity

$$Q = \dot{h} + v_\infty \dot{\theta} + v_\infty \sigma \tan \Lambda + b \left( \frac{1}{2} - a \right) (\dot{\theta} + v_\infty \tau \tan \Lambda)$$

which occurs in the terms associated with the wake. The net result of these considerations is that the circulatory-flow velocity potential may be regarded as determined.

The pressure difference between upper and lower surfaces of the wing at a point  $x$  is (positive downward)

$$\begin{aligned} p &= -2\rho \left( \frac{\partial \phi}{\partial t} + v \frac{\partial \phi}{\partial \xi} \right) \\ &= -2\rho \left( \frac{\partial \phi}{\partial t} + v \frac{\partial \phi}{\partial x'} \cos \Lambda + v \frac{\partial \phi}{\partial y'} \sin \Lambda \right) \end{aligned} \quad (5a)$$

where  $\phi$  is in general the total potential (the sum of circulatory-flow and noncirculatory-flow potentials). The last term in equation (5a) is the product of the component of main-stream velocity taken along the wing and the lengthwise change in the velocity potential and is often neglected even in steady-flow work. The question of the retention or neglect of this last term seems partly dependent on the order in which the approximations are introduced—specifically, whether velocity potentials for the whole flow pattern are found and then the integrated forces are determined or whether section forces are first determined and then integrated. It seems appropriate to retain at least the noncirculatory part  $\phi_N$  of  $\phi$  in the last term of equation (5a). In view, however, of the nature of the approximate treatment of the circulatory potential and of the inherent shortcomings of a strip analysis, in particular the neglect of lengthwise variations in wake vortex strength, complicating the results by also including  $\phi_r$  in this term does not appear worth while. (This neglect of  $\phi_r$  and retention of  $\phi_N$  is realized to involve some inconsistencies in that account may not be taken of other higher order terms associated with lengthwise variation of the wing wake, which may be of the same order as terms retained.) Thus equation (5a) becomes

$$p = -2\rho \left( \frac{\partial \phi}{\partial t} + v \frac{\partial \phi}{\partial x'} \cos \Lambda + v \frac{\partial \phi_N}{\partial y'} \sin \Lambda \right) \quad (5b)$$

For harmonic motion in each degree of freedom, relations for the pressure may be integrated over the chord to yield expressions for the air forces and moments. For the sake of separating and identifying the terms in force and moment expressions which are due solely to the inclusion of the last term in equation (5b), a special bracket  $\{ \}$  is employed. Thus these terms may be readily omitted. Numerical checks among the calculations made for the present report showed the effect of inclusion of the last term in equation (5b) on the calculated results to be quite small, even for  $60^\circ$  of sweepback within the range of other parameters investigated.

The expressions for the aerodynamic lift (positive down) and for the moment about the elastic axis (positive leading edge up), each per unit length of the wing, are as follows:

$$\begin{aligned} P &= -2\pi\rho v_\infty b C \left[ \dot{h} + v_\infty \dot{\theta} + v_\infty \dot{\sigma} \tan \Lambda + b \left( \frac{1}{2} - a \right) (\dot{\theta} + v_\infty \dot{\tau} \tan \Lambda) \right] - \\ &\quad \pi\rho b^2 \left[ \ddot{h} + v_\infty \ddot{\theta} + v_\infty \ddot{\sigma} \tan \Lambda + \{ v_\infty \ddot{\sigma} \tan \Lambda + v_\infty^2 \dot{\tau} \tan \Lambda + v_\infty^2 \frac{\partial \sigma}{\partial y'} \tan^2 \Lambda \} \right] + \\ &\quad \pi\rho b^3 a \left[ \ddot{\theta} + v_\infty \ddot{\tau} \tan \Lambda + \{ v_\infty \ddot{\tau} \tan \Lambda + v_\infty^2 \frac{\partial \tau}{\partial y'} \tan^2 \Lambda \} \right] \end{aligned} \quad (6)$$

$$\begin{aligned} M_a &= 2\pi\rho v_\infty b^2 \left( \frac{1}{2} + a \right) C \left[ \dot{h} + v_\infty \dot{\theta} + v_\infty \dot{\sigma} \tan \Lambda + b \left( \frac{1}{2} - a \right) (\dot{\theta} + v_\infty \dot{\tau} \tan \Lambda) \right] - \\ &\quad \pi\rho v_\infty b^3 \left[ \left( \frac{1}{2} - a \right) \dot{\theta} + \frac{1}{2} v_\infty \dot{\tau} \tan \Lambda \right] + \pi\rho b^3 a \left[ \ddot{h} + v_\infty \ddot{\sigma} \tan \Lambda + \right. \\ &\quad \left. \{ v_\infty \ddot{\sigma} \tan \Lambda + v_\infty^2 \dot{\tau} \tan \Lambda + v_\infty^2 \frac{\partial \sigma}{\partial y'} \tan^2 \Lambda \} \right] - \pi\rho b^4 \left( \frac{1}{8} + a^2 \right) \left[ \ddot{\theta} + \right. \\ &\quad \left. v_\infty \ddot{\tau} \tan \Lambda + \{ v_\infty \ddot{\tau} \tan \Lambda + v_\infty^2 \frac{\partial \tau}{\partial y'} \tan^2 \Lambda \} \right] \end{aligned} \quad (7)$$

where

$$C = C(k_n) = F(k_n) + iG(k_n)$$

is the function associated with the wake developed by Theodorsen in reference 5; the reduced frequency parameter  $k_n$  is defined by

$$k_n = \frac{\omega b}{v_n} = \frac{\omega b}{v \cos \Lambda} \quad (8)$$

As has already been stated, the foregoing expressions were developed and apply for steady sinusoidal oscillations,

$$\left. \begin{aligned} h &= h_1(y') e^{i\omega t} \\ \theta &= \theta_1(y') e^{i\omega t} \end{aligned} \right\} \quad (9)$$

The amplitude, velocity, and acceleration in each degree of freedom are related as in the degree of freedom  $h$ ; that is,

$$\begin{aligned} \dot{h} &= i\omega h \\ \ddot{h} &= -\omega^2 h \end{aligned}$$

**Expressions for force and moment.**—With the use of such relations, equations (6) and (7) may be put into the form

$$P = -\pi \rho b^3 \omega^2 (h B_{ch} + \theta B_{c\theta}) \quad (10a)$$

$$M_a = -\pi \rho b^4 \omega^2 (h B_{ah} + \theta B_{a\theta}) \quad (11a)$$

where

$$\begin{aligned} B_{ch} &= \frac{1}{b} A_{ch} + \frac{\sigma}{h} \tan \Lambda \left( -i \frac{1}{k_n} \right) ([-1] + A_{ch}) + \\ &\quad \left[ \frac{b}{h} \frac{\partial \sigma}{\partial y'} \tan^2 \Lambda \left( \frac{1}{k_n^2} \right) \right] \\ B_{c\theta} &= A_{c\alpha} + \frac{\tau}{\theta} b \tan \Lambda (A_{cr}) + \left[ \frac{b^2}{\theta} \frac{\partial \tau}{\partial y'} \tan^2 \Lambda \left( -\frac{a}{k_n^2} \right) \right] \\ B_{ah} &= \frac{1}{b} A_{ah} + \frac{\sigma}{h} \tan \Lambda \left( -i \frac{1}{k_n} \right) ([a] + A_{ah}) + \\ &\quad \left[ \frac{b}{h} \frac{\partial \sigma}{\partial y'} \tan^2 \Lambda \left( -\frac{a}{k_n^2} \right) \right] \\ B_{a\theta} &= A_{a\alpha} + \frac{\tau}{\theta} b \tan \Lambda (A_{ar}) + \left[ \frac{b^2}{\theta} \frac{\partial \tau}{\partial y'} \tan^2 \Lambda \left( \frac{1}{8} + a^2 \right) \frac{1}{k_n^2} \right] \end{aligned}$$

in which the four following coefficients:

$$\begin{aligned} A_{ch} &= -1 - \frac{2G}{k_n} + i \frac{2F}{k_n} \\ A_{c\alpha} &= a + \frac{2F}{k_n^2} - \left( \frac{1}{2} - a \right) \frac{2G}{k_n} + i \left[ \frac{1}{k_n} + \frac{2G}{k_n^2} + \left( \frac{1}{2} - a \right) \frac{2F}{k_n} \right] \\ A_{ah} &= a + \left( \frac{1}{2} + a \right) \frac{2G}{k_n} + i \left( \frac{1}{2} + a \right) \left( -\frac{2F}{k_n} \right) \\ &= -\frac{1}{2} - \left( \frac{1}{2} + a \right) A_{ch} \\ A_{a\alpha} &= -\frac{1}{8} - a^2 - \left( \frac{1}{2} + a \right) \frac{2F}{k_n^2} + \left( \frac{1}{4} - a^2 \right) \frac{2G}{k_n} + \\ &\quad i \left[ \left( \frac{1}{2} - a \right) \frac{1}{k_n} - \left( \frac{1}{4} - a^2 \right) \frac{2F}{k_n} - \left( \frac{1}{2} + a \right) \frac{2G}{k_n^2} \right] \end{aligned}$$

are identical with those used in the case of the unswept wing. Additionally,

$$\begin{aligned} A_{cr} &= \left[ \frac{1}{k_n^2} \right] - i \frac{1}{k_n} \left[ \frac{1}{2} + [a] + \left( \frac{1}{2} - a \right) A_{ch} \right] \\ A_{ar} &= -i \frac{1}{k_n} \left[ -\left( \frac{3}{8} + \left[ \frac{1}{8} + a^2 \right] \right) + i \frac{1}{k_n} \left( \frac{1}{2} - [a] \right) - \left( \frac{1}{4} - a^2 \right) A_{ch} \right] \end{aligned}$$

It is of interest to note that equations (6) and (7) reduce, for the case of the wing in steady flow ( $k_n = 0$ ), to

$$\begin{aligned} P &= -2\pi \rho b v_n^2 \left[ \theta + \sigma \tan \Lambda + \tau b \tan \Lambda \left( \left[ \frac{1}{2} \right] + \frac{1}{2} - a \right) + \right. \\ &\quad \left. \left[ \frac{b}{2} \frac{\partial \sigma}{\partial y'} \tan^2 \Lambda - \frac{a}{2} b^2 \frac{\partial \tau}{\partial y'} \tan^2 \Lambda \right] \right] \quad (10b) \end{aligned}$$

$$\begin{aligned} M_a &= 2\pi \rho b^2 v_n^2 \left[ (\theta + \sigma \tan \Lambda) \left( \frac{1}{2} + a \right) + \tau a b \tan \Lambda \left( \left[ \frac{1}{2} \right] - a \right) + \right. \\ &\quad \left. \left[ \frac{a b}{2} \frac{\partial \sigma}{\partial y'} \tan^2 \Lambda - \frac{1}{2} b^2 \left( \frac{1}{8} + a^2 \right) \frac{\partial \tau}{\partial y'} \tan^2 \Lambda \right] \right] \quad (11b) \end{aligned}$$

per unit length of wing.

**Introduction of modes.**—Equations (10a) and (11a) give the total aerodynamic force and moment on a segment of a sweptback wing oscillating in a simple harmonic manner. Relations for mechanical equilibrium applicable to a wing segment may be set up, but it is preferable to bring in directly the three-dimensional-mode considerations. (See for example, reference 6.) This end may be readily accomplished by the combined use of Rayleigh type approximations and the classical methods of Lagrange. The vibrations at flutter are assumed to consist of a combination of fixed mode shapes, each mode shape representing a degree of freedom associated with a generalized coordinate. The total mechanical energy, the potential energy, and the work done by applied forces, aerodynamic and structural, are then obtained by the integration of the section characteristics over the span. The Rayleigh type approximation enters in the representation of the potential energy in terms of the uncoupled frequencies.

As is customary, the modes are introduced into the problem as varying sinusoidally with time. For the purpose of simplicity of analysis, one bending degree of freedom and one torsion degree of freedom are carried through in the present development. Actually, any number of degrees of freedom may be added if desired, exactly as with an unswept wing. Let the mode shapes be represented by

$$\left. \begin{aligned} h &= [f_h(y')] \underline{h} \\ \theta &= [f_\theta(y')] \underline{\theta} \end{aligned} \right\} \quad (12)$$

where  $\underline{h} = h_0 e^{i\omega t}$  is the generalized coordinate in the bending degree of freedom, and  $\underline{\theta} = \theta_0 e^{i\omega t}$  is the generalized coordinate in the torsion degree of freedom. (In a more general treatment the mode shapes must be solved, but in this procedure  $f_h(y')$  and  $f_\theta(y')$  are chosen, ordinarily as real functions of  $y'$ . Complex functions may be used to represent twisted modes.) The constants  $h_0$  and  $\theta_0$  are in general complex and thus signify the phase difference between the two degrees of freedom.

In the subsequent treatment the reader will notice that in some expressions, namely for force and moment,  $h$  and  $\theta$  can conveniently and logically be retained in their complex form. In other expressions, notably for energy, one is forced to utilize  $h$  and  $\theta$  as real quantities. Appropriate statements will be made where necessary.

For each degree of freedom an equation of equilibrium may be obtained from Lagrange's equation

$$\frac{d}{dt} \left( \frac{\partial T}{\partial \dot{q}_i} \right) - \frac{\partial T}{\partial q_i} + \frac{\partial U}{\partial q_i} = Q_i \quad (13)$$

where  $q_i$  is a generalized coordinate and  $Q_i$  is the corresponding generalized force. The kinetic energy of the mechanical system is

$$T = \frac{1}{2} \dot{h}^2 \int_0^{l'} m [f_h(y')]^2 dy' + \frac{1}{2} \dot{\theta}^2 \int_0^{l'} I_a [f_\theta(y')]^2 dy' + \dot{h} \dot{\theta} \int_0^{l'} m x_a b [f_h(y')] [f_\theta(y')] dy' \quad (14)$$

where  $h$  and  $\theta$  here and in the subsequent equations (15) are to be interpreted as real in order that the energy be always positive (or zero), and for definiteness can be regarded as the real parts of  $h e^{i\omega t}$  and  $\theta e^{i\omega t}$  respectively; and where

$m$  mass of wing per unit length, slugs per foot  
 $I_a$  mass moment of inertia of wing about its elastic axis per unit length, slug-feet<sup>2</sup> per foot  
 $x_a b$  distance of sectional center of gravity from the elastic axis, positive rearward, feet

The potential energy of the mechanical system may be expressed in a form not involving bending-torsion cross-stiffness terms:

$$U = \frac{1}{2} \dot{h}^2 \int_0^{l'} EI \left( \frac{d^2 f_h}{dy'^2} \right)^2 dy' + \frac{1}{2} \dot{\theta}^2 \int_0^{l'} GJ \left( \frac{df_\theta}{dy'} \right)^2 dy' \quad (15a)$$

where

$EI$  bending stiffness, pound-feet<sup>2</sup>  
 $GJ$  torsional stiffness, pound-feet<sup>2</sup>

If Rayleigh type approximations are used to introduce frequency, the expression for the potential energy may be written in a more convenient form:

$$U = \frac{1}{2} \omega_h^2 \dot{h}^2 \int_0^{l'} m f_h^2 dy' + \frac{1}{2} \omega_a^2 \dot{\theta}^2 \int_0^{l'} I_a f_\theta^2 dy' \quad (15b)$$

Another expression for the potential energy is

$$U = \frac{1}{2} \dot{h}^2 \int_0^{l'} C_h f_h^2 dy' + \frac{1}{2} \dot{\theta}^2 \int_0^{l'} C_a f_\theta^2 dy' \quad (15c)$$

The effective spring constants  $C_h$  and  $C_a$  correspond to unit length of wing and thus conform to their use in references 5 to 7. The constants are effectively defined by

$$\omega_h^2 = \frac{\int_0^{l'} C_h f_h^2 dy'}{\int_0^{l'} m f_h^2 dy'} \quad \omega_a^2 = \frac{\int_0^{l'} C_a f_\theta^2 dy'}{\int_0^{l'} I_a f_\theta^2 dy'}$$

These effective spring constants are related to the frequencies associated with the chosen modes. For so-called uncoupled

modes the frequencies appropriate to pure modes (obtained by proper constraints) are often used. On the other hand, employment of the normal or natural modes and frequencies appropriate to them, which might be obtained by proper ground test or by calculation, may be preferred. In either case the convenience of not having cross-stiffness terms in the potential-energy expression is noted.

Application is now made to obtain the equation of equilibrium in the bending degree of freedom. Equation (13) becomes

$$\frac{d}{dt} \left( \frac{\partial T}{\partial \dot{h}} \right) - \frac{\partial T}{\partial h} + \frac{\partial U}{\partial h} = Q_h \quad (16)$$

The term  $Q_h$  represents all the bending forces not derivable from the potential-energy function and consists of the aerodynamic forces together with the structural damping forces. The virtual work  $\delta W$  done on the wing by these forces as the wing moves through the virtual displacements  $\delta h$  and  $\delta \theta$  is

$$\begin{aligned} \delta W &= \int_0^{l'} \left[ \left( P - C_h \frac{g_h}{\omega} \dot{h} \right) \delta h + \left( M_a - C_a \frac{g_a}{\omega} \dot{\theta} \right) \delta \theta \right] dy' \\ &= \int_0^{l'} \left( P - m \omega_h^2 \frac{g_h}{\omega} f_h \dot{h} \right) f_h dy' \delta h + \\ &\quad \int_0^{l'} \left( M_a - I_a \omega_a^2 \frac{g_a}{\omega} f_\theta \dot{\theta} \right) f_\theta dy' \delta \theta = Q_h \delta h + Q_\theta \delta \theta \end{aligned} \quad (17)$$

where

$g_h$  structural damping coefficient for bending vibration  
 $g_a$  structural damping coefficient for torsional vibration

In this expression the aerodynamic forces appropriate to sinusoidal oscillations are used. The application of the structural damping as in equation (17) (proportional to deflection and in phase with velocity) corresponds to the manner in which it is introduced in reference 7. In accordance with the preceding development, the aerodynamic and structural damping forces and moments in equation (17) are regarded as complex, but the virtual displacements  $\delta h$  and  $\delta \theta$  should be considered real. Thus, the physically significant part of the resulting expression for virtual work is the real part. Since the subsequent analysis reverts to expressions for forces and moments, no further qualifications on the use of  $h$  and  $\theta$  in their convenient complex forms are needed.

For the half-wing

$$\begin{aligned} Q_h &= \int_0^{l'} \left( P - m \omega_h^2 \frac{g_h}{\omega} f_h \dot{h} \right) f_h dy' \\ &= -\pi \rho b^3 \omega^2 \int_0^{l'} \left( \frac{b}{b_r} \right)^3 \left[ \frac{h}{b} A_{ca} f_h^2 + \frac{h}{b} \left( -i \frac{1}{k_n} \right) \{ (-1) + \right. \\ &\quad \left. A_{ca} (\tan \Lambda) f_h \frac{df_h}{dy'} + \left[ \frac{h}{b} \frac{1}{k_n^2} b (\tan^2 \Lambda) f_h \frac{d^2 f_h}{dy'^2} \right] + \right. \\ &\quad \left. \frac{\theta A_{ca} f_\theta f_h + \theta A_{cr} b (\tan \Lambda) f_h \frac{df_\theta}{dy'} + \right. \\ &\quad \left. \left[ \theta \left( -\frac{a}{k_n^2} \right) b^2 (\tan^2 \Lambda) f_h \frac{d^2 f_\theta}{dy'^2} \right] + \frac{h}{b} \frac{1}{k_n} i \left( \frac{\omega_h}{\omega} \right)^2 g_h f_h^2 \right] dy' \end{aligned} \quad (18)$$

where  $b_r$  is the semichord at some reference section. Performance of the operations indicated in equation (16) and collection of terms lead to the equation of equilibrium in the bending degree of freedom

$$\left( \frac{1}{b_r} \left[ 1 - \left( \frac{\omega_h}{\omega} \right)^2 (1 + i g_h) \right] \frac{1}{b_r} \int_0^{l'} \left( \frac{b}{b_r} \right)^2 \frac{1}{\kappa} f_h^2 dy' - \frac{1}{b_r} \int_0^{l'} \left( \frac{b}{b_r} \right)^2 A_{ch} f_h^2 dy' + \int_0^{l'} \left( \frac{b}{b_r} \right)^3 \tan \Lambda \left( i \frac{1}{k_n} \right) \{ -1 \} + A_{ch} f_h \frac{df_h}{dy'} dy' - \left[ b_r \int_0^{l'} \left( \frac{b}{b_r} \right)^4 \tan^2 \Lambda \left( \frac{1}{k_n^2} \right) f_h \frac{d^2 f_h}{dy'^2} dy' \right] \right\} + \left\{ \int_0^{l'} \left( \frac{b}{b_r} \right)^3 \left( \frac{x_a}{\kappa} - A_{ca} \right) f_h f_\theta dy' - b_r \int_0^{l'} \left( \frac{b}{b_r} \right)^4 A_{cr} (\tan \Lambda) f_h \frac{df_\theta}{dy'} dy' + \left[ b_r^2 \int_0^{l'} \left( \frac{b}{b_r} \right)^5 \frac{a}{k_n^2} \tan^2 \Lambda f_h \frac{d^2 f_\theta}{dy'^2} dy' \right] \right\} \pi \rho b_r^3 \omega^2 = 0 \quad (19a)$$

where

$$\frac{1}{\kappa} = \frac{m}{\pi \rho b^2}$$

By a parallel development the equation of equilibrium for the torsional degree of freedom may also be obtained as follows:

$$\left( \frac{1}{b_r} \left\{ \frac{1}{b_r} \int_0^{l'} \left( \frac{b}{b_r} \right)^3 \left( \frac{x_a}{\kappa} - A_{ah} \right) f_h f_\theta dy' + \int_0^{l'} \left( \frac{b}{b_r} \right)^4 \tan \Lambda \left( i \frac{1}{k_n} \right) \{ a \} + A_{ah} f_\theta \frac{df_h}{dy'} dy' + \left[ b_r \int_0^{l'} \left( \frac{b}{b_r} \right)^5 \tan^2 \Lambda \left( \frac{a}{k_n^2} \right) f_\theta \frac{d^2 f_h}{dy'^2} dy' \right] \right\} + \frac{1}{b_r} \left\{ \left[ 1 - \left( \frac{\omega_a}{\omega} \right)^2 (1 + i g_a) \right] \int_0^{l'} \left( \frac{b}{b_r} \right)^4 \frac{r_a^2}{\kappa} f_\theta^2 dy' - \int_0^{l'} \left( \frac{b}{b_r} \right)^4 A_{aa} f_\theta^2 dy' - b_r \int_0^{l'} \left( \frac{b}{b_r} \right)^5 \tan \Lambda (A_{ar}) f_\theta \frac{df_\theta}{dy'} dy' - \left[ b_r^2 \int_0^{l'} \left( \frac{b}{b_r} \right)^6 \tan^2 \Lambda \left( \frac{1}{8} + a^2 \right) \frac{1}{k_n^2} f_\theta \frac{d^2 f_\theta}{dy'^2} dy' \right] \right\} \right\} \pi \rho b_r^4 \omega^2 = 0 \quad (20a)$$

where  $r_a = \sqrt{I_a/m b^2}$  (radius of gyration of wing about the elastic axis).

**Determinantal equation for flutter.**—Equations (19a) and (20a) may be rewritten with the use of the nondimensional coordinate  $\eta = \frac{y'}{l'}$ . They then are in the form

$$(hA_2 + gB_2) \pi \rho b_r^3 \omega^2 = 0 \quad (19b)$$

$$(hD_2 + gE_2) \pi \rho b_r^4 \omega^2 = 0 \quad (20b)$$

where

$$\begin{aligned} A_2 &= \left[ 1 - \left( \frac{\omega_h}{\omega} \right)^2 (1 + i g_h) \right] \frac{l'}{b_r} \int_0^{1.0} \left( \frac{b}{b_r} \right)^2 \frac{1}{\kappa} [F_h(\eta)]^2 d\eta - \frac{l'}{b_r} \int_0^{1.0} \left( \frac{b}{b_r} \right)^2 A_{ch} [F_h(\eta)]^2 d\eta + \\ &\quad \int_0^{1.0} \left( \frac{b}{b_r} \right)^3 \tan \Lambda \left( i \frac{1}{k_n} \right) \{ -1 \} + A_{ch} [F_h(\eta)] \frac{dF_h}{d\eta} d\eta - \left\{ \frac{b_r}{l'} \int_0^{1.0} \left( \frac{b}{b_r} \right)^4 \tan^2 \Lambda \left( \frac{1}{k_n^2} \right) [F_h(\eta)] \frac{d^2 F_h}{d\eta^2} d\eta \right\} \\ B_2 &= l' \int_0^{1.0} \left( \frac{b}{b_r} \right)^3 \left( \frac{x_a}{\kappa} - A_{ca} \right) [F_h(\eta)] [F_\theta(\eta)] d\eta - b_r \int_0^{1.0} \left( \frac{b}{b_r} \right)^4 \tan \Lambda (A_{cr}) [F_h(\eta)] \frac{dF_\theta}{d\eta} d\eta + \\ &\quad \left\{ \frac{b_r^2}{l'} \int_0^{1.0} \left( \frac{b}{b_r} \right)^5 \tan^2 \Lambda \left( \frac{a}{k_n^2} \right) [F_h(\eta)] \frac{d^2 F_\theta}{d\eta^2} d\eta \right\} \\ D_2 &= \frac{l'}{b_r} \int_0^{1.0} \left( \frac{b}{b_r} \right)^3 \left( \frac{x_a}{\kappa} - A_{ah} \right) [F_\theta(\eta)] [F_h(\eta)] d\eta + \int_0^{1.0} \left( \frac{b}{b_r} \right)^4 \tan \Lambda \left( i \frac{1}{k_n} \right) \{ a \} + A_{ah} [F_\theta(\eta)] \frac{dF_h}{d\eta} d\eta + \\ &\quad \left\{ \frac{b_r}{l'} \int_0^{1.0} \left( \frac{b}{b_r} \right)^5 \tan^2 \Lambda \left( \frac{a}{k_n^2} \right) [F_\theta(\eta)] \frac{d^2 F_h}{d\eta^2} d\eta \right\} \\ E_2 &= l' \left[ 1 - \left( \frac{\omega_a}{\omega} \right)^2 (1 + i g_a) \right] \int_0^{1.0} \left( \frac{b}{b_r} \right)^4 \frac{r_a^2}{\kappa} [F_\theta(\eta)]^2 d\eta - l' \int_0^{1.0} \left( \frac{b}{b_r} \right)^4 A_{aa} [F_\theta(\eta)]^2 d\eta - \\ &\quad b_r \int_0^{1.0} \left( \frac{b}{b_r} \right)^5 \tan \Lambda (A_{ar}) [F_\theta(\eta)] \frac{dF_\theta}{d\eta} d\eta - \left\{ \frac{b_r^2}{l'} \int_0^{1.0} \left( \frac{b}{b_r} \right)^6 \tan^2 \Lambda \left( \frac{1}{8} + a^2 \right) \frac{1}{k_n^2} [F_\theta(\eta)] \frac{d^2 F_\theta}{d\eta^2} d\eta \right\} \end{aligned}$$

in which  $F_h(\eta) = f_h(l'\eta)$  and  $F_\theta(\eta) = f_\theta(l'\eta)$ .

The borderline condition of flutter, separating damped and undamped oscillations, is determined from the nontrivial solution of the simultaneous homogeneous equations (19b) and (20b). Such a solution corresponds to the fact that mechan-



ical equilibrium exists for sinusoidal oscillations at a certain airspeed and with a certain frequency. The flutter condition thus is given by the vanishing of the determinant of the coefficients

$$\begin{vmatrix} A_2 & B_2 \\ D_2 & E_2 \end{vmatrix} = 0$$

Application to the case of uniform, cantilever swept wings is made in the next section.

#### APPLICATION TO UNIFORM CANTILEVER SWEPT WINGS

The first step in the application of the theory is to assume or develop the deflection functions to be used. For the purpose of applying the analysis to the wing models employed in the experiments it appeared reasonable to use for the deflection functions,  $F_b(\eta)$  and  $F_t(\eta)$ , the uncoupled first bending and first torsion mode shapes of an ideal uniform cantilever beam. Although approximations for these mode shapes could be used, the analysis utilized the exact expressions developed from equations (120) and (106d), respectively, of reference 8 by application of appropriate boundary conditions.

The bending-mode shape can be written

$$F_b(\eta) = C_1 \left[ \frac{\sinh \beta_1 + \sin \beta_1}{\cosh \beta_1 + \cos \beta_1} (\cos \beta_1 \eta - \cosh \beta_1 \eta) + \sinh \beta_1 \eta - \sin \beta_1 \eta \right]$$

where  $\beta_1 = 0.5969\pi$  for first bending. The torsion mode shape can be written

$$F_t(\eta) = C_2 \sin \beta_2 \eta$$

where  $\beta_2 = \frac{\pi}{2}$  for first torsion and  $C_1$  and  $C_2$  are constants.

The integrals appearing in the determinant elements  $A_2$ ,  $B_2$ ,  $D_2$ , and  $E_2$  are

$$\int_0^{1.0} F_b^2 d\eta = 1.8554 C_1^2$$

$$\int_0^{1.0} F_t^2 d\eta = 0.5000 C_2^2$$

$$\int_0^{1.0} F_b \frac{dF_b}{d\eta} d\eta = 3.7110 C_1^2$$

$$\int_0^{1.0} F_t \frac{dF_t}{d\eta} d\eta = 0.3183 C_2^2$$

$$\int_0^{1.0} F_b \frac{d^2 F_b}{d\eta^2} d\eta = 1.5926 C_1^2$$

$$\int_0^{1.0} F_t \frac{d^2 F_t}{d\eta^2} d\eta = -1.2337 C_2^2$$

$$\int_0^{1.0} F_b F_t d\eta = \int_0^{1.0} F_t F_b d\eta = -0.9233 C_1 C_2$$

$$\int_0^{1.0} F_b \frac{dF_t}{d\eta} d\eta = -1.4040 C_1 C_2$$

$$\int_0^{1.0} F_t \frac{dF_b}{d\eta} d\eta = -2.0669 C_1 C_2$$

$$\int_0^{1.0} F_b \frac{d^2 F_t}{d\eta^2} d\eta = 2.2782 C_1 C_2$$

$$\int_0^{1.0} F_t \frac{d^2 F_b}{d\eta^2} d\eta = -1.4722 C_1 C_2$$

The flutter determinant becomes

$$\begin{vmatrix} 1.8554C_1\frac{l'}{b_r}A + 3.7110C_1^2\left(i\frac{1}{k_n}\right)([-1] + A_{ch})\tan\Lambda - \left[1.5926C_1^2\frac{\tan^2\Lambda}{l'/b_r}\frac{1}{k_n^2}\right] & -0.9233C_1C_2l'B - (-1.4040C_1C_2)b_rA_{cr}\tan\Lambda + \left[2.2782C_1C_2b_r\frac{\tan^2\Lambda}{l'/b_r}\frac{a}{k_n^2}\right] \\ -0.9233C_1C_2\frac{l'}{b_r}D - 2.0669C_1C_2\left(i\frac{1}{k_n}\right)([a] + A_{ah})\tan\Lambda + \left[-1.4722C_1C_2\frac{\tan^2\Lambda}{l'/b_r}\frac{a}{k_n^2}\right] & 0.5000C_2^2l'E - 0.3183C_2^2b_rA_{ar}\tan\Lambda - \left[-1.2337C_2^2b_r\frac{\tan^2\Lambda}{l'/b_r}\left(\frac{1}{8} + a^2\right)\frac{1}{k_n^2}\right] \end{vmatrix} = 0$$

or more conveniently, when columns and rows of the determinant are divided by appropriate terms

$$\begin{vmatrix} A + 2.0000\frac{\tan\Lambda}{l'/b_r}\left(i\frac{1}{k_n}\right)([-1] + A_{ch}) - \left[0.85837\left(\frac{\tan\Lambda}{l'/b_r}\right)^2\frac{1}{k_n^2}\right] & B - 1.5206\frac{\tan\Lambda}{l'/b_r}A_{cr} - \left[2.4675\left(\frac{\tan\Lambda}{l'/b_r}\right)^2\frac{a}{k_n^2}\right] \\ 0.9189D + 2.0571\frac{\tan\Lambda}{l'/b_r}\left(i\frac{1}{k_n}\right)([a] + A_{ah}) + \left[1.4652\left(\frac{\tan\Lambda}{l'/b_r}\right)^2\frac{a}{k_n^2}\right] & E - 0.63660\frac{\tan\Lambda}{l'/b_r}A_{ar} + \left[2.4675\left(\frac{\tan\Lambda}{l'/b_r}\right)^2\left(\frac{1}{8} + a^2\right)\frac{1}{k_n^2}\right] \end{vmatrix} = 0$$

where

$$A = \frac{1}{\kappa} \left[ 1 - \left( \frac{\omega_h}{\omega} \right)^2 (1 + i g_h) \right] - A_{ch}$$

$$B = \frac{x_\alpha}{\kappa} - A_{c\alpha}$$

$$D = \frac{x_\alpha}{\kappa} - A_{ah}$$

$$E = \frac{r_\alpha^2}{\kappa} \left[ 1 - \left( \frac{\omega_\alpha}{\omega} \right)^2 (1 + i g_\alpha) \right] - A_{a\alpha}$$

It is interesting to note that the parameters  $\Lambda$  and  $l'/b_r$  appear only in the combination  $\frac{\tan\Lambda}{l'/b_r}$  in the immediately preceding determinant. The solution of the determinant results in the flutter condition.

## EXPERIMENTAL INVESTIGATION

## APPARATUS

**Wind tunnel.**—The tests were conducted in the Langley 4.5-foot flutter research tunnel which is of the closed-throat, single-return type employing either air or Freon-12 as a testing medium at pressures varying from 4 inches of mercury to 30 inches of mercury. In Freon-12, the speed of sound is 324 miles per hour and the density is 0.0106 slug per cubic foot at standard pressure and temperature. The maximum choking Mach number for these tests was approximately 0.92. The Reynolds number range was from  $0.26 \times 10^6$  to  $2.6 \times 10^6$  with most of the tests at Reynolds numbers of the order of  $1.0 \times 10^6$ .

**Models.**—In order to obtain structural parameters required for the flutter studies, different types of construction were used for the models. Some models were solid spruce, others were solid balsa, and many were combinations of balsa with various aluminum-alloy inserts. Seven series of models were investigated, for which the cross sections and plan forms are shown in figure 2.

Figure 2 (a) shows the series of models which were swept back by shearing the cross sections parallel to the air stream. In order to obtain flutter with these low-aspect-ratio models, thin sections and relatively light and weak wood construction were employed.

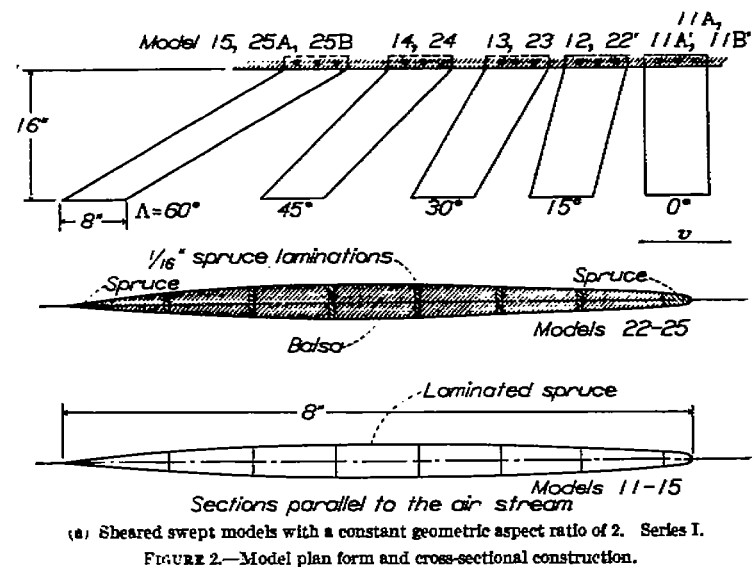


FIGURE 2.—Model plan form and cross-sectional construction.

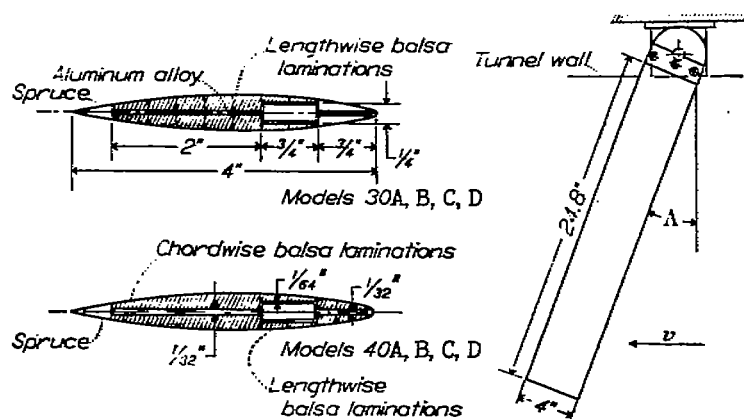


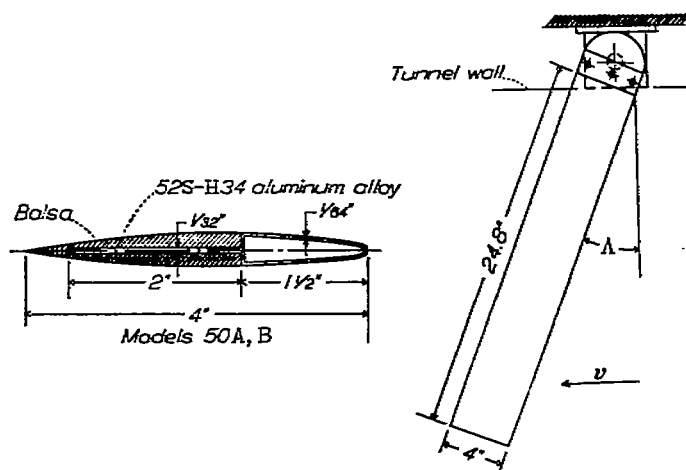
FIGURE 2.—Continued.

The series of rectangular-plan-form models shown in figure 2 (b) were swept back by using a base mount that could be rotated to give the desired sweep angle. The same base mount was used for testing models at forward sweep angles. It is known that for forward sweep angles divergence is critical. In an attempt to separate the divergence and flutter speeds in the sweepforward tests, a D-spar cross-sectional construction was used to get the elastic axis relatively far forward (fig. 2 (c)).

Two series of wings (figs. 2 (d) and 2 (e)) were swept back with the length-chord ratios kept constant. In these series of models, the chord perpendicular to the leading edge was kept constant and the bases were aligned parallel to the air stream. The wings of length-chord ratio 8.5 (fig. 2 (d)) were cut down to get the wings of length-chord ratio 6.5 (fig. 2 (e)).

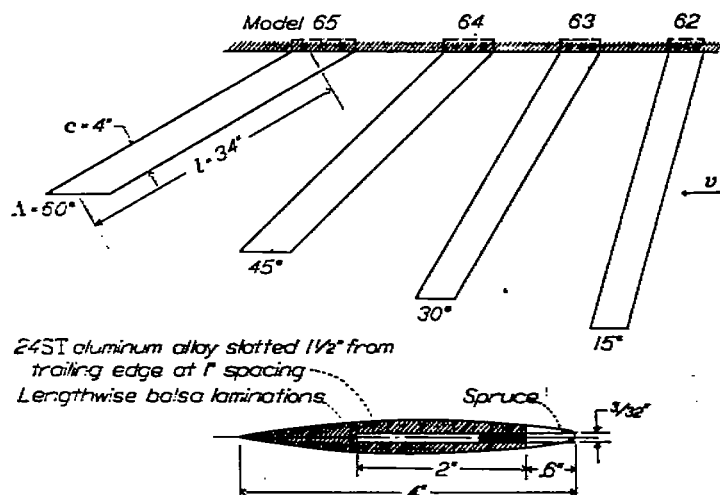
Another series of models obtained by using this same manner of sweep (fig. 2 (f)) was used for investigating some effects of tip shape.

Spanwise strips of lead were fastened to the models shown in figure 2 (e) and a series of tests were conducted with these weighted models to determine the effect of center-of-gravity shift on the flutter speed of swept wings. The method of



(c) Models in which a rotating mount is used to determine the effect of sweepback and sweepforward on the critical velocity. Series III.

FIGURE 2.—Continued.



(d) Swept models having a length-chord ratio of 8.5. Series IV.

FIGURE 2.—Continued.

varying the center of gravity is shown in figure 2 (g). In order to obtain data at zero sweep angle it was necessary, because of the proximity of flutter speed to wing-divergence speed, to use three different wings. These zero-sweep-angle wings, of 8-inch chord and 48-inch length, had an internal weight system.

The models were mounted from the top of the tunnel as cantilever beams with rigid bases (fig. 3). Near the root of each model two sets of strain gages were fastened, one set for recording principally bending deformations and the other set for recording principally torsional deflections.

#### METHODS

**Determination of model parameters.**—Pertinent geometric and structural properties of the model are given in tables I to VII. Some parameters of interest are discussed in the following paragraphs.

As an indication of the nearness to sonic-flow conditions, the critical Mach number is listed. This Mach number is determined by the Kármán-Tsien method for a wing section normal to the leading edge at zero lift.

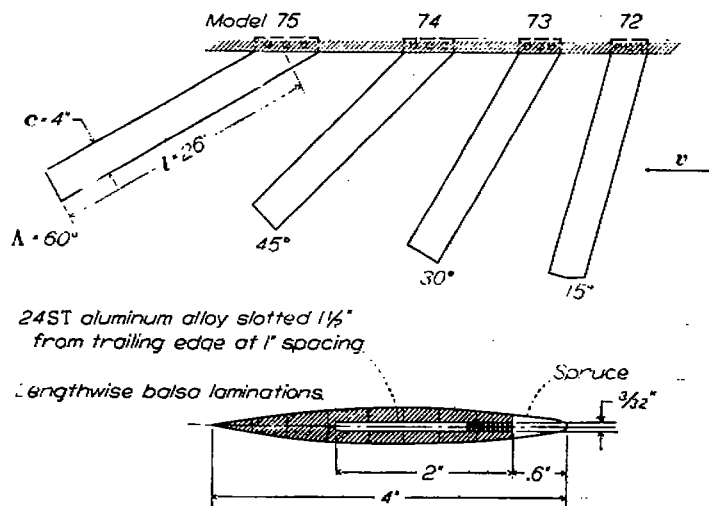
The geometric aspect ratio of a wing is here defined as

$$A_z = \frac{\text{Semispan}^2}{\text{Plan-form area}} = \frac{(l \cos \Lambda)^2}{lc} = \frac{l}{c} \cos^2 \Lambda = \frac{A}{2}$$

The geometric aspect ratio  $A_z$  is used in place of the conventional aspect ratio  $A$  because the models were only semispan wings. For sheared swept wings, obtained from a given unswept wing, the geometric aspect ratio is constant, whereas for the wings of constant length-chord ratio the geometric aspect ratio decreases with  $\cos^2 \Lambda$  as the angle of sweep is increased.

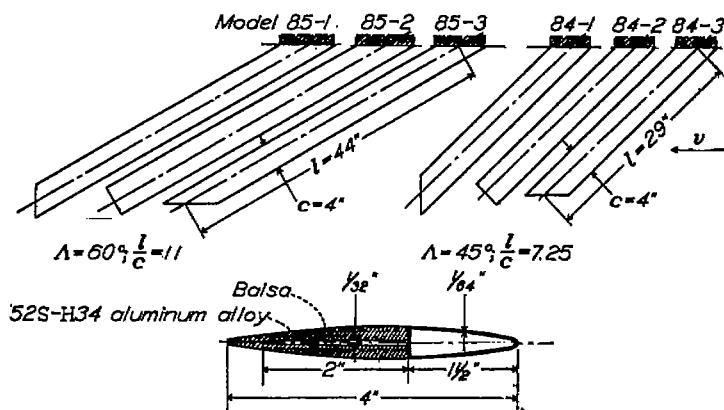
The weight, center-of-gravity position, and polar moment of inertia of the models were determined by usual means. The models were statically loaded at the tip to obtain the rigidities in torsion and bending  $GJ$  and  $EI$ .

A parameter occurring in the methods of analysis of this report is the position of the elastic axis. A "section" elastic axis located at  $x_{ea}$  was obtained for wings from each series of models as follows: The wings were clamped at the root normal to the leading edge and at a chosen spanwise station



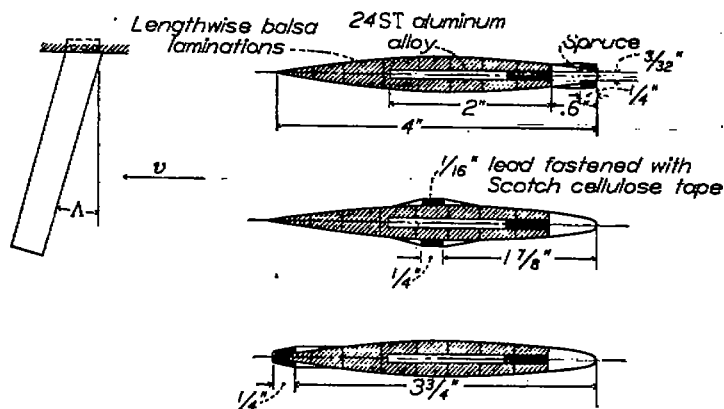
(e) Swept models having a length-chord ratio of 6.5. Series V.

FIGURE 2.—Continued.



(f) Models used to investigate the effect of tip shape on the flutter velocity. Series VI

FIGURE 2.—Continued.



Model	$\Lambda$ (deg)
91-1, 91-2, 91-3 *	0
92-1, 92-2, 92-3	15
93-1, 93-2, 93-3	30
94-1, 94-2, 94-3	45
95-1, 95-2, 95-3	60

\* Chord=8", lead inside balsa.

(g) Models used to determine the effect of center-of-gravity shift on the flutter velocity of swept wings. Series VII.

FIGURE 2.—Concluded.



FIGURE 3.—Model 12 in the tunnel test section.

were loaded at points lying in the chordwise direction. The point for which pure bending deflection occurred, with no twist in the plane normal to the leading edge, was determined. The same procedure was used for those wings which were clamped at the root, not normal, but at an angle to the leading edge. A different elastic axis designated the "wing" elastic axis and located at  $x_{ea}'$  was thus determined.

For these uniform, swept wings with fairly large length-chord ratios, the wing elastic axis was reasonably straight and remained essentially parallel to the section elastic axis, although it was found to move farther behind the section elastic axis as the angle of sweep was increased. It is realized that in general for nonuniform wings—for example, wings with cut-outs or skewed clamping—a certain degree of cross stiffness exists and the concept of an elastic axis is an oversimplification. More general concepts such as those involving influence coefficients may be required. These more strict considerations, however, are not required here since the elastic-axis parameter is of fairly secondary importance.

The wing mass-density ratio  $\kappa$  is the ratio of the mass of a cylinder of testing medium, of a diameter equal to the chord of the wing, to the mass of the wing, both taken for unit length along the wing. The density of the testing medium when flutter occurred was used in the evaluation of  $\kappa$ .

**Determination of the reference flutter speed.**—It is convenient in presenting and comparing data of swept and unswept wings to employ a certain reference flutter speed. This reference flutter speed will serve to reduce variations in flutter characteristics which arise from changes in the various model parameters such as density and section properties not pertinent to the investigation. It thus aids in systematizing the data and emphasizing the desired effects of sweep including effects of aspect ratio and Mach number.

This reference flutter speed  $V_R$  may be obtained in the following way. Suppose the wing to be rotated about the intersection of the elastic axis with the root to a position of zero sweep. In this position the reference flutter speed is calculated by the method of reference 7, which assumes an idealized, uniform, infinite wing mounted on springs in an incompressible medium. For nonuniform wings, a reference section taken at a representative spanwise position, or some integrated value, may be used. Since the wings used were uniform, any reference section will serve. The reference flutter speed may thus be considered a "section" reference flutter speed and parameters of a section normal to the leading edge are used in its calculation. This calculation also employs the uncoupled first bending and torsion frequencies of the wing (obtained from the measured frequencies) and the measured density of the testing medium at time of flutter. The calculation yields a corresponding reference flutter frequency which is useful in comparing the frequency data. For the sake of completeness a further discussion of the reference flutter speed is given in appendix B.

**Test procedure and records.**—Since flutter is often a sudden and destructive phenomenon, coordinated test procedures were required. During each test, the tunnel speed was slowly raised until a speed was reached for which the

amplitudes of oscillation of the model in bending and torsion increased rapidly while the frequencies in bending and torsion, as observed on the screen of the recording oscillograph, merged to the same value. At this instant, the tunnel conditions were recorded and an oscillograph record of the model deflections was taken. The tunnel speed was immediately reduced in an effort to prevent destruction of the model.

From the tunnel data, the experimental flutter speed  $V_e$ , the density of the testing medium  $\rho$ , and the Mach number  $M$  were determined. No blocking or wake corrections to the measured tunnel velocity were applied.

From the oscillogram the experimental flutter frequency  $f_e$  and the phase difference  $\phi$  (or the phase difference  $\pm 180^\circ$ ) between the bending and torsion deflections near the root were read. A reproduction of a typical oscillograph flutter record, which indicated the flutter to be a coupling of the wing bending and torsion degrees of freedom, is shown as figure 4. Since semispan wings mounted rigidly at the base were used, the flutter mode may be considered to correspond to the flutter of a complete wing having a very heavy fuselage at midspan—that is, to the symmetrical type.

The natural frequencies of the models in bending and torsion at zero airspeed were recorded before and after each test in order to ascertain possible changes in structural characteristics. In most cases there were no appreciable changes in frequencies but there were some reductions in stiffnesses for models which had been weakened by fluttering violently. Analysis of the decay records of the natural frequencies indicated that the wing damping coefficients  $g_b$  and  $g_a$  (reference 7) were about 0.02 in the first bending mode and 0.03 in the torsion mode.

## RESULTS AND DISCUSSION

### EXPERIMENTAL INVESTIGATION

**Presentation of experimental data.**—Results of the experimental investigation are listed in detail in tables I to VII, and some significant experimental trends are illustrated

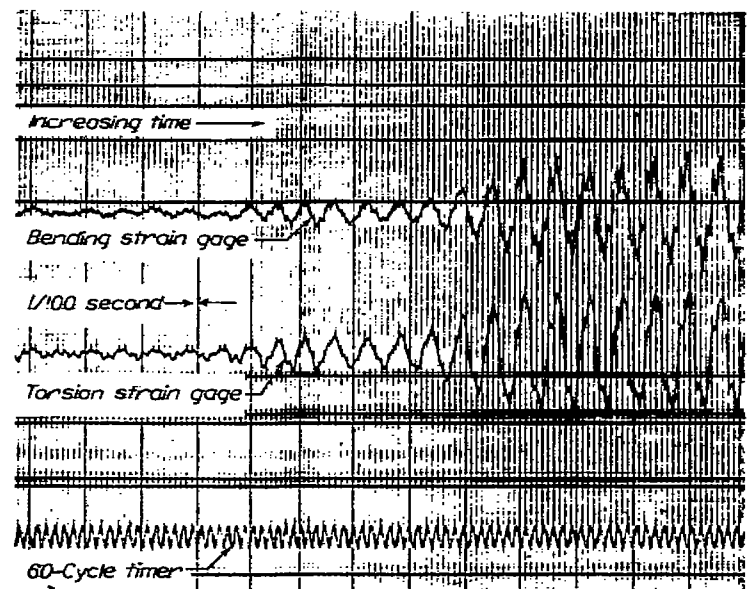


FIGURE 4.—Oscillograph record of model at flutter.

in figures 5 to 10. As a basis for presenting and comparing the test results, the ratio of experimental tunnel stream conditions to the reference flutter conditions is employed so that the data indicate more clearly combined effects of aspect ratio, sweep, and Mach number. As previously mentioned, use of the reference flutter speed  $V_R$  serves to reduce variations in flutter characteristics which arise from changes in other parameters, such as density and section properties, which are not pertinent to this investigation. (See appendix B.)

**Some effects on flutter speed.**—A typical plot showing the effect of compressibility on the flutter speed of wings at various angles of sweepback is shown in figure 5. These data are from tests of the rectangular-plan-form models (type 30) that were swept back by use of the rotating mount, for which arrangement the reference flutter speed does not vary with either Mach number or sweep angle. Observe the large increase in speed ratio at the high sweep angles.

The data of reference 1 from tests of a rigid, flexibly mounted rectangular model having a rotating base are also plotted in figure 5. It can be seen that the data from the cantilever models of the present report which had a similar method of sweep are in conformity with the data from the flexibly mounted model. This indicates that, for uniform wings having the range of parameters involved in these tests, the differences due to mode shape are not very great.

Figure 6 is a cross plot of the data from figure 5 plotted against  $\Lambda$  at a Mach number approximately equal to 0.65. The data of the swept wings of constant length-chord ratio and of the sheared swept wings are also included for comparison. The velocity ratio  $V_e/V_R$  is relatively constant at small sweep angles but rises noticeably at the large sweep angles. It is pointed out that the reference flutter speed  $V_R$  may be considered to correspond to a horizontal line at  $\frac{V_e}{V_R} = 1$  for the rotated and constant-length-chord-ratio wings, but for the sheared wings this reference speed corresponds to a curve decreasing somewhat less rapidly than  $\sqrt{\cos \Lambda}$  as  $\Lambda$  increases. (See appendix B.)

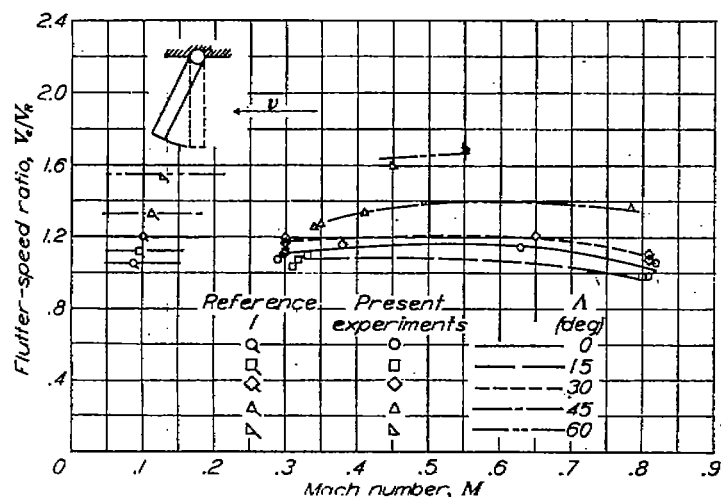


FIGURE 5.—Ratio of experimental to reference flutter speed as a function of Mach number for various sweep angles for series II models (fig. 2 (b)) on the rotating mount.

The order of magnitude of some three-dimensional effects may be noted from the fact that the shorter wings ( $\frac{l}{c} = 6.5$ , fig. 6, series V) have higher velocity ratios than the longer wings ( $\frac{l}{c} = 8.5$ , series IV). This increase may be due partly to differences in flutter modes as well as aerodynamic effects.

**Some effects on flutter frequency.**—Figure 7 is a representative plot of the flutter-frequency data given in table II. The figure shows the variation in flutter-frequency ratio with Mach number for different values of sweep angle for the models rotated back on the special mount. The ordinate

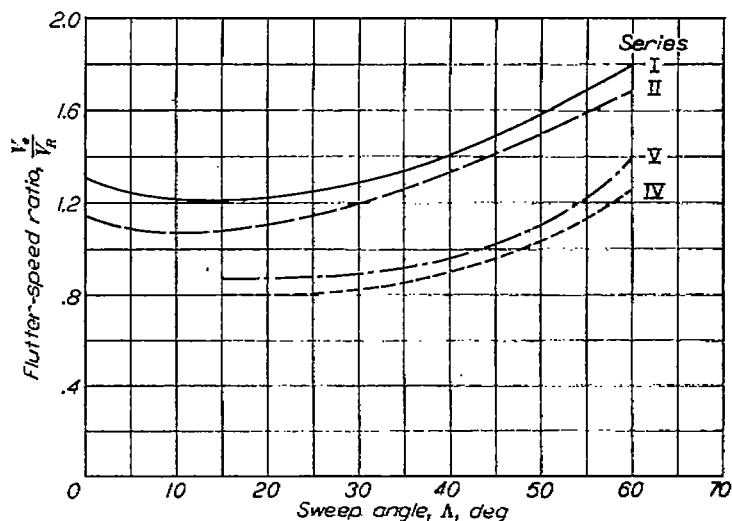
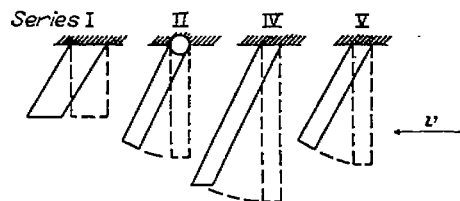


FIGURE 6.—Cross plot of ratio of experimental to reference flutter speed as a function of sweep angle for various wings. Mach number is approximately 0.65.

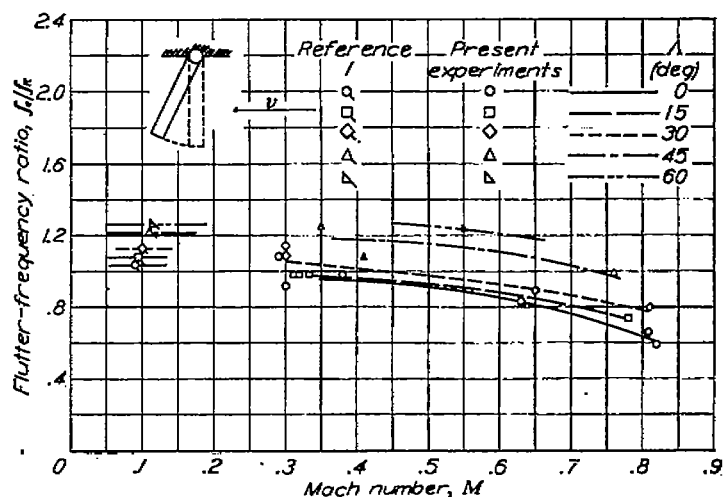


FIGURE 7.—Ratio of experimental to reference flutter frequency as a function of Mach number for various sweep angles for series II models (fig. 2 (b)) on the rotating mount.

is the ratio of the experimental flutter frequency to the reference flutter frequency  $f_e/f_R$ . It appears that there is a reduction in flutter frequency with increase in Mach number and also an increase in flutter frequency with increase in sweep. The data from reference 1 show the same trend with increase in sweep. Considerably more scatter may be noted in the frequency data than in the speed data (fig. 5) from the same tests.

The results of the tests for rotated wings with chordwise laminations (models 40A, B, C, D) are given in table II. At sweep angles up to  $30^\circ$  the values of the speed ratio  $V_e/V_R$  for wings of this construction were low (in the neighborhood of 0.9), and the flutter frequency ratios  $f_e/f_R$  were high (of the order of 1.4). As these results indicate and as visual observation showed, these models fluttered in a mode that apparently involved an appreciable proportion of the second bending mode. The models with spanwise laminations (models 30A, B, C, D) also showed indications of this higher flutter mode at low sweep angles; however, these models were able to pass through the small speed range of higher mode flutter without sufficiently violent oscillations to cause failure. At a still higher speed these models with spanwise laminations fluttered in a lower mode resembling a coupling of the torsion and first bending modes. This lower mode type of flutter characterized the flutter of both the sheared and constant-length-chord-ratio models.

For those wing models having the sheared type of balsa construction (models 22', 23, 24, and 25), the results are more difficult to compare with those of the other models. This difficulty arises chiefly because the lightness of the wood produced relatively high mass-density ratios  $\kappa$  and partly because of the nonhomogeneity of the mixed wood construction. For high values of  $\kappa$  the flutter-speed coefficient changes rather abruptly even for the unswept models (reference 7). The data are nevertheless included in table I.

**Effect of shift in center-of-gravity position on the flutter speed of swept wings.**—Results of the investigation of the effects of center-of-gravity shift on the flutter speed of swept wings are illustrated in figure 8. This figure is a cross plot of the experimental indicated air speeds as a function of sweep angle for various center-of-gravity positions. The ordinate is the experimental indicated air speed  $V_e \sqrt{\frac{\rho}{0.00238}}$ , which serves to reduce the scatter resulting from flutter tests at different densities of testing medium. The data were taken in the Mach number range between 0.14 and 0.44, so that compressibility effects are presumably negligible. As in the case of unswept wings, forward movement of the center of gravity increases the flutter speed. Again, the flutter speed increases with increase in the angle of sweep.

The models tested at zero sweep angle (models 91-1, 91-2, 91-3) were of different construction from and of larger size than the models tested at the higher sweep angles. Because of the manner of plotting the results, namely as experimental indicated airspeed (fig. 8), a comparison of the results of tests at  $\Lambda=0^\circ$  with the results of the tests of swept models

is not particularly significant. The points at zero sweep angle are included, however, to show that the increase in flutter speed due to a shift in the center-of-gravity position for the swept models is of the same order of magnitude as for the unswept models. For the unswept models, the divergence speed  $V_D$  and the reference flutter speed  $V_R$  are fairly near each other, and although the models appeared to flutter, the proximity of the flutter speed to the divergence speed may have influenced the value of the critical speed.

The method used to vary the center of gravity (see fig. 2 (g)) produced two bumps on the airfoil surface. At the low Mach numbers of these tests, however, the effect of this roughness on the flutter speed is considered negligible. For proper interpretation of figure 8, the fact must be kept in mind that the method of varying the location of the center of gravity changed the radius of gyration  $r_a$  and the torsional frequency  $f_a$ .

**The effect of sweepforward on the critical speed.**—An attempt was made to determine the variation in flutter speed with angle of sweepforward by testing wings on the mount that could be rotated both backward and forward. As expected, however, the model tended to diverge at forward sweep angles in spite of the relatively forward position of the elastic axis in this D-spar wing.

Figure 9 shows a plot of the ratio of critical speed to the reference flutter speed  $V_R$  against sweep angle  $\Lambda$ . Note the different curves for the sweptback and for the sweptforward conditions and the sharp reduction in critical speed as the

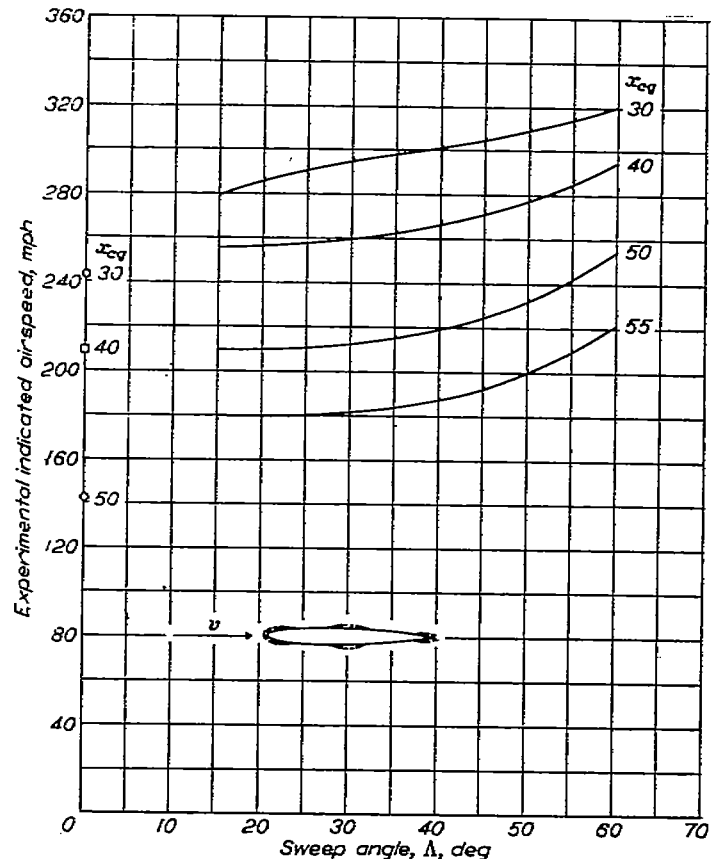


FIGURE 8.—Cross plot of flutter speed as a function of sweep angle for several center-of-gravity positions. Series VII models (fig. 2 (g)). Length-chord ratio is approximately 6.

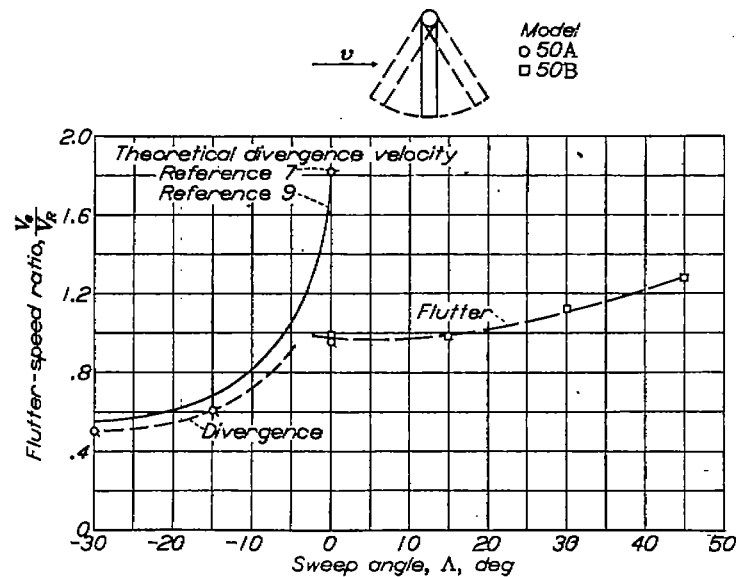


FIGURE 9.—Comparison of sweepforward and sweepback tests on wings tested on a rotating mount. Series III models (fig. 2 (c)).

angle of sweepforward is increased. The different curves result from two different phenomena. When the wing was swept back, it fluttered; whereas at forward sweep angles it diverged before the flutter speed was reached. Superposed on this plot for the negative values of sweep are the results of calculations based on an analytical study of divergence (reference 9). Reasonable agreement exists between theory and experiment at forward sweep angles. The small difference between the theoretical and experimental results may perhaps be due to an inaccuracy in determining either the position of the elastic axis of the model or the required slope of the lift curve or both.

The divergence speed  $V_D$  for the wing at zero sweep angle, as calculated by the simplified theory of reference 7, is also plotted in figure 9. This calculation is based on the assumption of a two-dimensional unswept wing in an incompressible medium. The values of the uncoupled torsion frequency and the density of the testing medium at time of flutter or divergence are employed. Reference 9 shows that a relatively small amount of sweepback raises the divergence speed sharply. For convenience, however, the numerical quantity  $V_D$  (based on the wing at zero sweep) is listed in table I for all the tests.

**Effect of tip modifications.**—Tests to investigate some of the over-all effects of tip shape were conducted and some results are shown in figure 10. Two sweep angles and two length-chord ratios were used in the experiments conducted at two Mach numbers. It is seen that, of the three tip shapes used, namely, tips perpendicular to the air stream, perpendicular to the wing leading edge, and parallel to the air stream, the wings with tips parallel to the air stream gave the highest flutter speeds.

#### DISCUSSION AND COMPARISON OF ANALYTICAL AND EXPERIMENTAL RESULTS

Correlation of analytical and experimental results has been made for wings swept back in the two different manners; that is, (1) sheared back with a constant value of  $A_z$ , and (2) rotated back. The two types of sheared wings (series I) and two rotated wings (models 30B and 30D) have been analyzed.

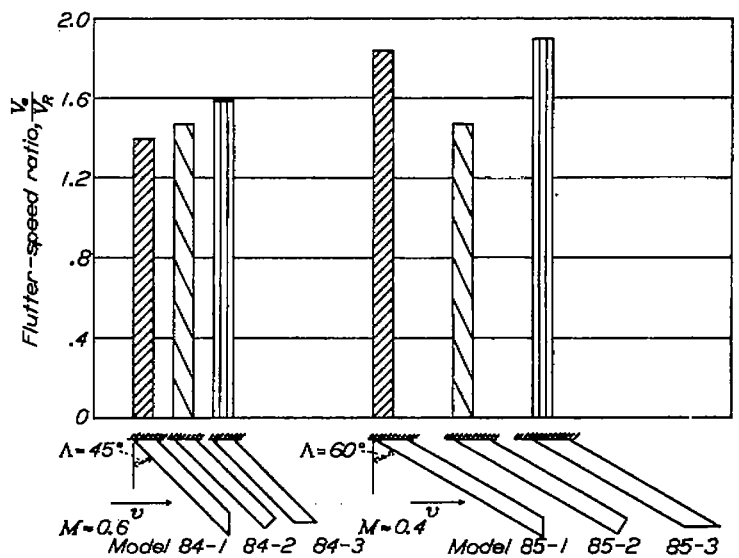


FIGURE 10.—Effect of tip shape on the flutter speed of swept wings. Wings of length-chord ratios of 7.25 and 11 (fig. 2 (f)). Series VI models.

Results of some solutions of the flutter determinant for a wing (model 30B) on a rotating base at several angles of sweepback are shown in figures 11 and 12. Figure 11 shows the flutter-speed coefficient as a function of the bending-to-torsion frequency ratio, and figure 12 shows the flutter frequency ratio as a function of the bending-to-torsion frequency ratio.

The calculated results (for those wings investigated analytically) are included in tables I and II. The ratios of experimental to analytical flutter speeds and flutter frequencies have been plotted against the angle of sweep in figures 13 to 16. If an experimental value coincides with the corresponding analytical predicted value, the ratio will fall at a value of 1.0 on the figures. Deviations of experimental results above or below the analytical results appear on the figures as ratios greater than or less than 1.0, respectively. The flutter-speed ratios plotted in figure 13 for the two rotated wings show very good agreement between analysis and experiment over the range of sweep angle,  $0^\circ$  to  $60^\circ$ . Such good agreement in both the trends and in the numerical quantities is gratifying but probably should not be expected in general. In view of the discussion of the last term in equation (5b) it may be of interest to mention that failure to include the terms arising from the last term of equation (5b) in the calculations for model 30B would decrease the ratio  $V/V_A$  corresponding to  $\Lambda=60^\circ$  by about 3 percent. The flutter frequency ratios of figure 14 obtained from the same two rotated wings are in good agreement.

The flutter-speed ratios plotted in figure 15 for the two types of sheared wings do not show such good conformity at the low angles of sweep, whereas for sweep angles beyond  $45^\circ$  the ratios are considerably nearer to 1.0. The sheared wings are again observed to have a constant value of  $A_z$  of 2.0 (aspect ratio for the whole wing would be 4.0). For this small value of aspect ratio the finite-span correction is appreciable at zero angle of sweep and, if made, would bring better agreement at that point. Analysis of the corrections for finite-span effects on swept wings requires further consideration.

Figures 13 and 15 also afford a comparison of the behavior of wings swept back in two manners: (1) rotated back with



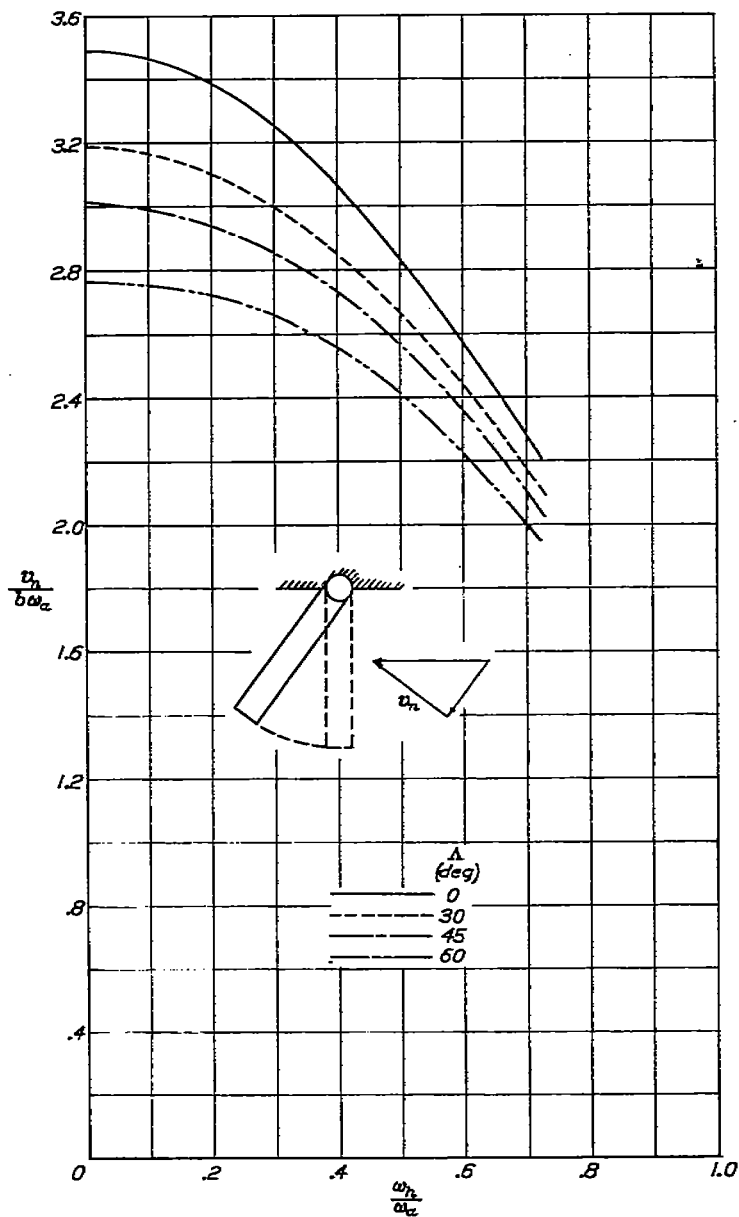


FIGURE 11.—Theoretical flutter-speed coefficient as a function of the ratio of bending to torsion frequency for the rotated model 30B at four angles of sweep and with a constant mass-density ratio ( $\frac{1}{\kappa}=37.8$ ).

constant length-chord ratio but decreasing aspect ratio (fig. 13), and (2) sheared back with constant aspect ratio and increasing length-chord ratio (fig. 15). A study of these two figures suggests that the length-chord ratio rather than the aspect ratio ( $\frac{\text{Span}^2}{\text{Area}}$ ) may be the relevant parameter in determining corrections for finite swept wings. (Admittedly, effects of tip shape and root condition are also involved and have not been precisely separated.)

Figure 16, which refers to the same sheared wings as figure 15, shows the ratios of experimental to predicted flutter frequencies. The trend is for the ratio to decrease as the angle of sweep increases. Table I shows that the flutter frequency  $f_B$  obtained with  $V_B$  and used as a reference in a previous section of the report is not significantly different from the frequency  $f_A$  predicted by the present analysis.

A few remarks can be made on estimates of over-all trends of the flutter speed of swept wings. As a first consideration the conclusion may be made that, if a rigid infinite yawed

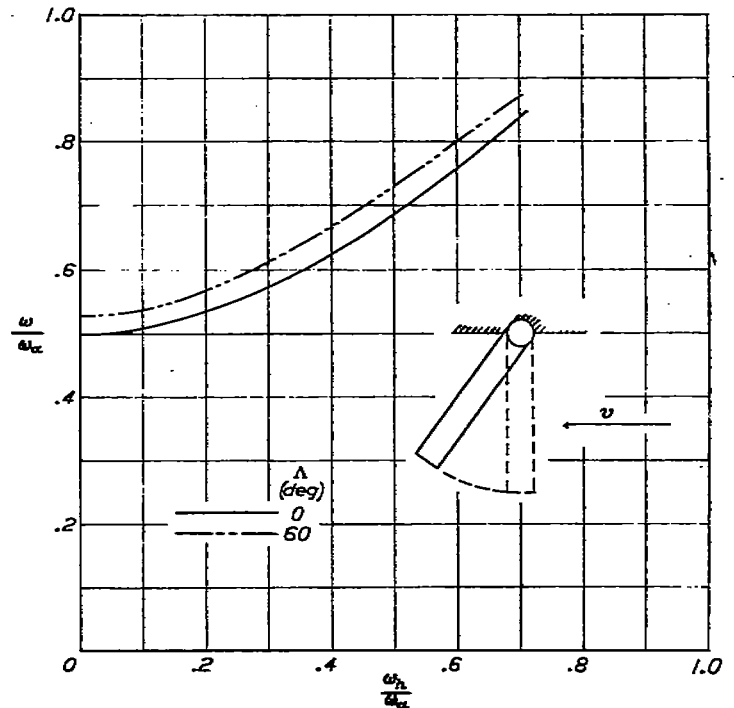


FIGURE 12.—Ratio of theoretical flutter frequency to torsional frequency as a function of the ratio of bending to torsion frequency for the rotated model 30B at two angles of sweep and with a constant mass-density ratio ( $\frac{1}{\kappa}=37.8$ ).

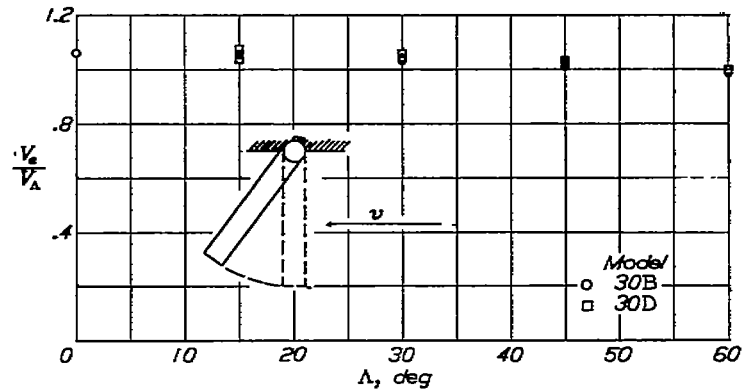


FIGURE 13.—Ratio of experimental to theoretically predicted flutter speed as a function of sweep angle for two rotated models.

wing were mounted on springs which permitted it to move vertically as a unit and to rotate about an elastic axis, the flutter speed would be proportional to  $1/\cos \Lambda$ . A finite yawed wing mounted on similar springs would be expected to have a flutter speed lying above the curve of  $1/\cos \Lambda$  because of finite-span effects. For a finite sweptback wing clamped at its root, however, the greater degree of coupling between bending and torsion adversely affects the flutter speed so as to bring the speed below the curve of  $1/\cos \Lambda$  for an infinite wing. This statement is illustrated in figure 17 which refers to a wing (model 30B) on a rotating base. The ordinate is the ratio of flutter speed at a given angle of sweep to the flutter speed calculated at zero angle of sweep. A theoretical curve is shown, together with experimentally determined points. Curves of  $1/\cos \Lambda$  and  $1/\sqrt{\cos \Lambda}$  are shown for convenience of comparison. The curve for model 30D (not shown in figure 17) also followed this trend quite closely. The foregoing remarks should prove useful for making estimates and discussing trends but are not intended to replace more complete calculation. In particular, mention may be made, for example, that a far-forward location

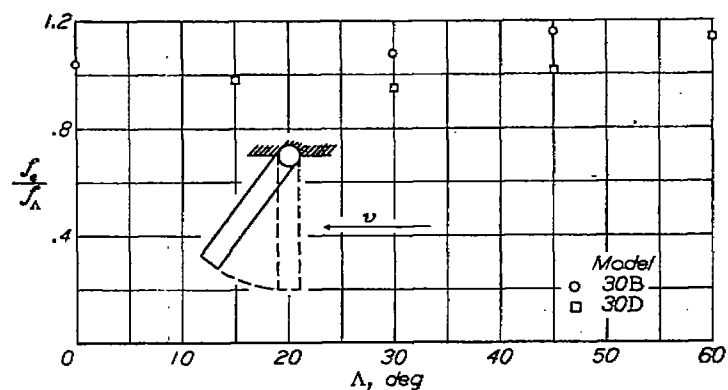


FIGURE 14.—Ratio of experimental to theoretically predicted flutter frequency as a function of sweep angle for two rotated models.

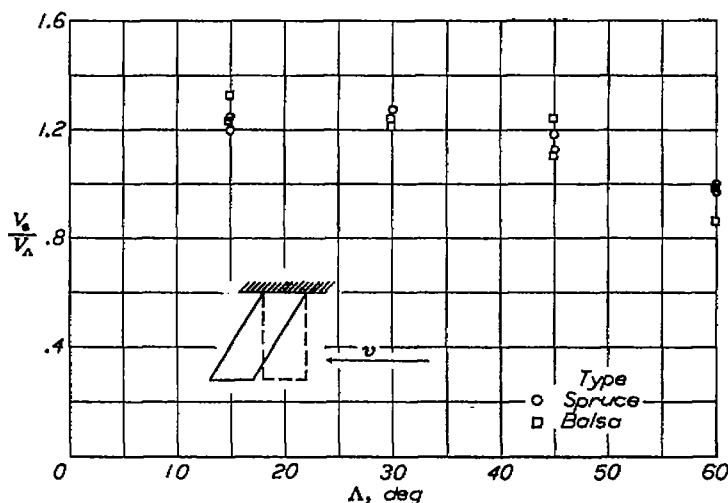


FIGURE 15.—Ratio of experimental to theoretically predicted flutter speed as a function of sweep angle for two types of sheared models.

of section center of gravity would lead to an entirely different trend. Moreover, as is apparent from the analysis, the bending stiffness can play an increasingly significant role with increase in the angle of sweep.

The experiments and calculations deal in general with wings having low ratios of natural first bending to first torsion frequencies. At high values of the ratio of bending frequency to torsion frequency, the position of the elastic axis becomes relatively more significant. Additional calculations to develop the theoretical trends are desirable.

### CONCLUSIONS

In a discussion and comparison of the results of an investigation of the flutter of a group of swept wings, the manner of sweep is significant. This report deals with two main groups of uniform, swept wings: rotated wings and sheared wings. In presenting the data, employment of a certain reference flutter speed was found convenient. The following conclusions seem to apply:

1. Comparison with experiment indicates that the analysis presented is satisfactory for giving the main effects of sweep, at least for nearly uniform cantilever wings of moderate length-chord ratios. Additional calculations are desirable to investigate various theoretical trends.

2. The coupling between bending and torsion adversely affects the flutter speed. The fact, however, that only a part of the forward velocity is aerodynamically effective

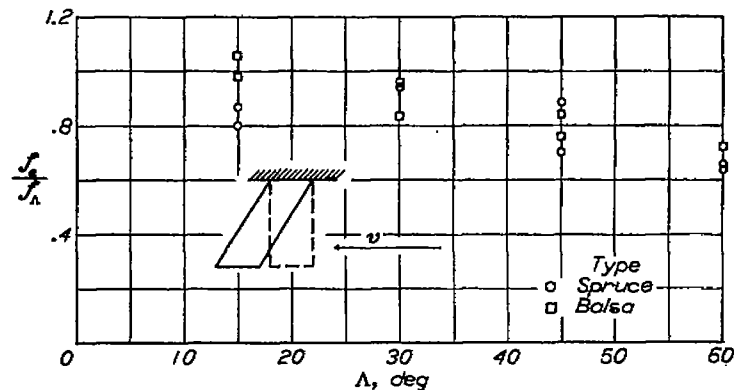


FIGURE 16.—Ratio of experimental to theoretically predicted flutter frequency as a function of sweep angle for two types of sheared wings.

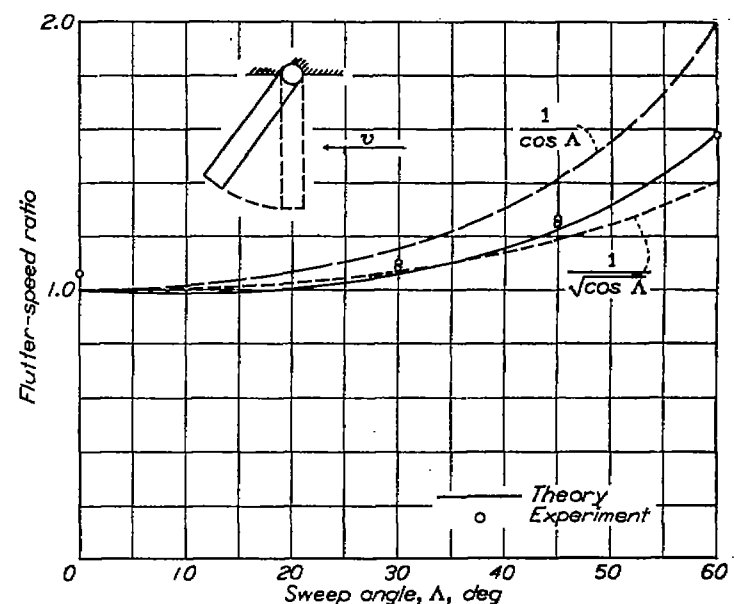


FIGURE 17.—Flutter-speed ratio as a function of sweep angle for model 30B at a constant mass-density ratio ( $\frac{\rho}{\rho_0} = 37.8$ ), showing analytical and experimental results.

increases the flutter speed. Certain approximate relations can be used to estimate some of the trends.

3. Although a precise separation of the effects of Mach number, aspect ratio, tip shape, and center-of-gravity position has not been accomplished, the order of magnitude of some of these combined effects has been experimentally determined. Experimental results indicated are

(a) The location of the section center of gravity is an important parameter and produces effects for swept wings similar to those for unswept wings over the range (30 percent to 70 percent chord) of locations tested.

(b) Appreciable differences in flutter speed have been found to be due to tip shape.

(c) The length-chord ratio of swept wings is a more relevant finite-span parameter than is the aspect ratio.

(d) Compressibility effects attributable to Mach number are fairly small, at least up to a Mach number of 0.8.

(e) The sweptforward wings could not be made to flutter but diverged before the flutter speed was reached.

LANGLEY AERONAUTICAL LABORATORY,  
NATIONAL ADVISORY COMMITTEE FOR AERONAUTICS,  
LANGLEY FIELD, VA., September 9, 1948.

## APPENDIX A

### THE EFFECT OF SWEEP ON THE FREQUENCIES OF A CANTILEVER BEAM

Early in the investigation it was decided to make an experimental vibration study of a simple beam at various sweep angles. The uniform, plate-like aluminum-alloy beam shown in figure 18 was used to make the study amenable to analysis. Length-chord ratios of 6, 3, and 1.5 were tested, the length  $l$  being defined as the length along the midchord. A single 60-inch beam was used throughout the investigation, the desired length and sweep angle being obtained by clamping the beam in the proper position with a  $1\frac{1}{2}$  by  $1\frac{1}{2}$  by 14-inch aluminum-alloy crossbar.

Figures 18 and 19 show the variation in modes and frequencies with sweep angle. In most cases, an increase in sweep angle increased the natural vibrational frequencies. As expected, the effect of sweep was more pronounced at the

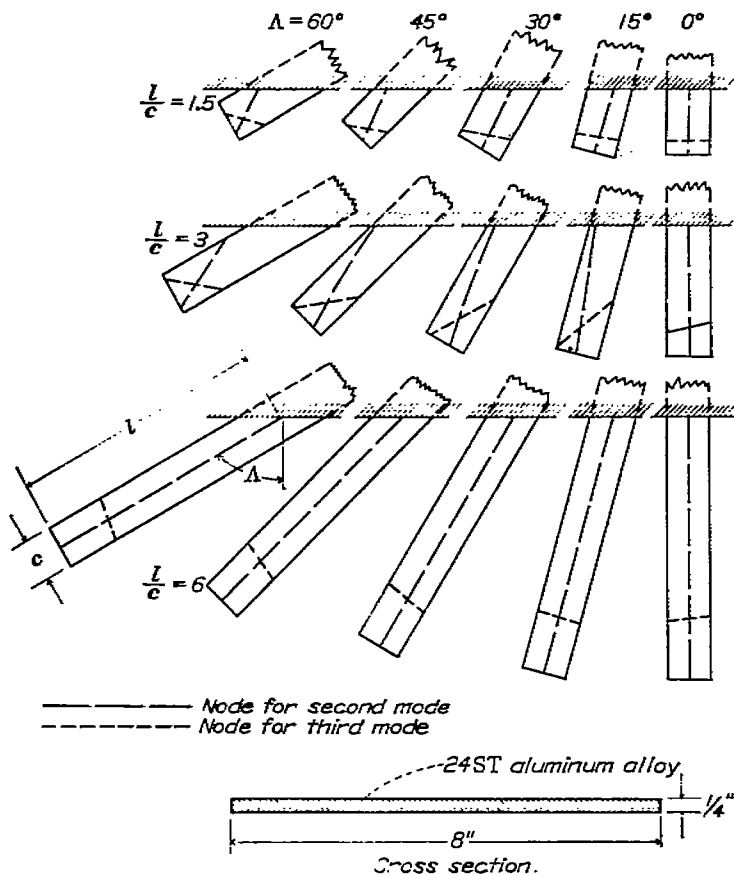


FIGURE 18.—Change in nodal lines with sweep and length-chord ratio for the vibration of an aluminum-alloy beam.

smaller values of length-chord ratio. The fundamental mode was found by striking the beam and measuring the frequency with a self-generating vibration pick-up and paper recorder. The second and third modes were excited by light-weight electromagnetic shakers clamped to the beam. These shakers were attached as close to the root as possible to give a node either predominantly spanwise or chordwise. The mode with the spanwise node, designated second mode, was primarily torsional vibration, whereas the mode with the chordwise node, designated third mode, was primarily a second bending vibration.

The first two bending frequencies and the lowest torsion frequency, determined analytically for a straight uniform unswept beam, are plotted in figure 19. Good agreement exists with the experimental results for the length-chord ratios of 6 and 3, but for a ratio of 1.5 (length equal to 12 inches and chord equal to 8 inches) less favorable agreement exists. This discrepancy may be attributed to the fact that the beam at the short length-chord ratio of 1.5 resembled more a plate than a beam and did not meet the theoretical assumptions of a perfectly rigid base and of simple-beam stress distributions. The data are valid for use in comparing the experimental frequencies of the beam when swept with the frequencies at zero sweep, which was the purpose of the test.

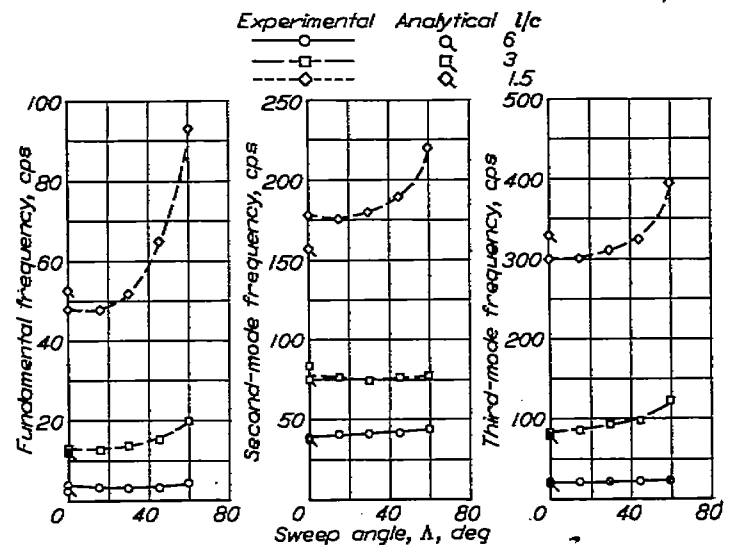


FIGURE 19.—Variation of frequencies with sweep and length-chord ratio for the vibration of an aluminum-alloy beam.

## APPENDIX B

### DISCUSSION OF THE REFERENCE FLUTTER SPEED

For use in comparing data of swept and unswept wings, a reference flutter speed  $V_R$  is convenient. This reference flutter speed is the flutter speed determined from the simplified theory of reference 7. This theory deals with two-dimensional unswept wings in incompressible flow and depends upon a number of wing parameters. The calculations in this report utilize parameters of sections perpendicular to the leading edge, first bending frequency, uncoupled torsion frequency, density of testing medium at time of flutter, and zero damping. Symbolically,

$$V_R = b \omega_\alpha f \left( \kappa, x_{cg}, x_{ca}, r_\alpha^2, \frac{f_h}{f_\alpha} \right)$$

**Variation in reference flutter speed with sweep angle for sheared swept wings.**—The reference flutter speed is independent of sweep angle for a homogeneous rotated wing and for homogeneous wings swept back by keeping the length-chord ratio constant. For a series of homogeneous wings swept back by the method of shearing, however, a definite variation in reference flutter speed with sweep angle exists since sweeping a wing by shearing causes a reduction in chord perpendicular to the wing leading edge and an increase in length along the midchord as the angle of sweep is increased. The resulting reduction in the mass-density-ratio parameter and first bending frequency tends to raise the reference flutter speed, whereas the reduction in semichord tends to lower the reference flutter speed as the angle of sweep is increased. The final effect upon the reference flutter speed depends on the other properties of the wing. The purpose of this section is to show the effect of these changes on the magnitude of the reference flutter speed for a series of homogeneous sheared wings having properties similar to those of the sheared swept models used in this report.

Let the subscript 0 refer to properties of the wing at zero sweep angle. The following parameters are then functions of the sweep angle:

$$b = b_0 \cos \Lambda$$

$$l = \frac{l_0}{\cos \Lambda}$$

Since  $m$  is proportional to  $b$ ,

$$\kappa = \frac{\pi \rho b^2}{m} = \kappa_0 \cos \Lambda$$

Similarly, since  $I$  is proportional to  $b$ ,

$$f_{h1} = \frac{0.56}{l^2} \sqrt{\frac{EI}{m}} = (f_{h1})_0 (\cos \Lambda)^2$$

Also, because  $f_\alpha$  is independent of  $\Lambda$ ,

$$\frac{f_{h1}}{f_\alpha} = \left( \frac{f_{h1}}{f_\alpha} \right)_0 (\cos \Lambda)^2$$

An estimate of the effect on the flutter speed of these changes in semichord and mass parameter with sweep angle may be obtained from the approximate formula given in reference 7,

$$V_R \approx b \omega_\alpha \sqrt{\frac{r_\alpha^2}{\kappa} \frac{0.5}{0.5 + a + x_\alpha}} = V_{R_0} \sqrt{\cos \Lambda}$$

This approximate analysis of the effect on the reference flutter speed does not depend upon the first bending frequency but assumes  $f_h/f_\alpha$  to be small.

In order to include the effect of changes in bending-torsion frequency ratio, a more complete analysis must be carried out. Figure 20 presents some results of a numerical analysis based on a homogeneous wing with properties at zero sweep angle as follows:

$$\begin{array}{ll} x_{cg} = 50 & b_0 = 0.333 \\ x_{ca} = 45 & \left( \frac{1}{\kappa} \right)_0 = 10 \\ r_\alpha^2 = 0.25 & \left( \frac{f_{h1}}{f_\alpha} \right)_0 = 0.4 \\ f_\alpha = 100 & \end{array}$$

In figure 20 the curve showing the decrease in  $V_R$  with  $\Lambda$  is slightly above the  $\sqrt{\cos \Lambda}$  factor indicated by the approximate formula.

**Effect of elastic-axis position on reference flutter speed.**—As pointed out in the definition of elastic axis, the measured

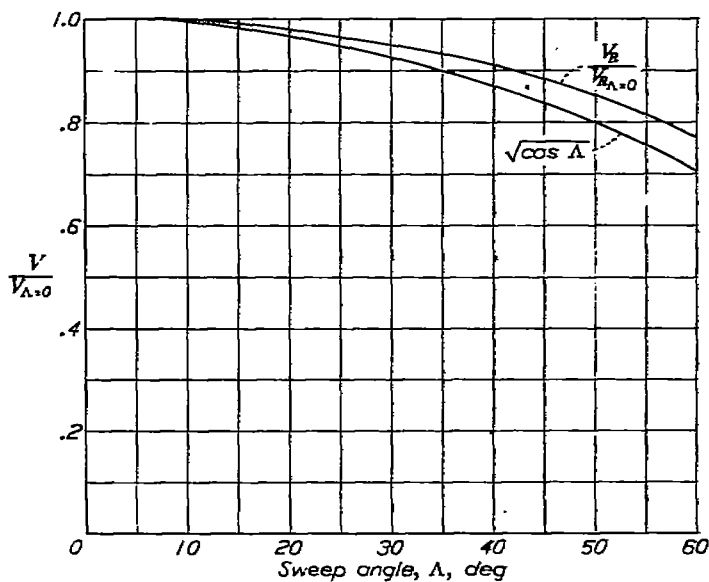


FIGURE 20.—Variation in reference flutter speed with sweep for sheared wings.

locus of elastic centers  $x_{ea}'$  fell behind the section elastic axis for the swept models with bases parallel to the air stream. In order to get an idea of the effect of elastic-axis position on the chosen reference flutter speed, computations were made both of  $V_R$  and a second reference flutter speed  $V_R'$  similar to  $V_R$  except that  $x_{ea}'$  was used in place of  $x_{ea}$ . The maximum difference between these two values of reference flutter speed was of the order of 7 percent. This difference occurred at a sweep angle of  $60^\circ$  when the wing elastic axis was farthest behind the section elastic axis. Thus, for wings of this type,

the reference flutter speed is not very sensitive to elastic-axis position. The reference flutter frequency  $f_R'$  was found in conjunction with  $V_R'$ . The maximum difference between  $f_R$  and  $f_R'$  was less than 10 percent. Thus, the convenient use of the reference flutter speed and reference frequency is not altered by these elastic-axis considerations.

## REFERENCES

1. Kramer, Edward H.: The Effect of Sweepback on the Critical Flutter Speed of Wings. MR No. TSEAC5-4595-2-5, Eng. Div., Air Technical Service Command, Army Air Forces, March 15, 1946.
2. Broadbent, E. G.: Some Considerations of the Flutter Problems of High-Speed Aircraft. Sec. International Aero. Conference, N. Y., 1949, pp. 556-581.
3. Fettis, Henry E.: Calculations of the Flutter Characteristics of Swept Wings at Subsonic Speeds. MR No. TSEAC5-4595-2-9, Air Materiel Command, Army Air Forces, May 13, 1946.
4. Spielberg, Irvin, Fettis, H. E., and Toney, H. S.: Methods for Calculating the Flutter and Vibration Characteristics of Swept Wings. MR No. MCREXA5-4595-8-4, Air Materiel Command, U. S. Air Force, Aug. 3, 1948.
5. Theodorsen, Theodore: General Theory of Aerodynamic Instability and the Mechanism of Flutter. NACA Rep. 496, 1935.
6. Smilg, Benjamin, and Wasserman, Lee S.: Application of Three-Dimensional Flutter Theory to Aircraft Structures. ACTR No. 4798, Materiel Div., Army Air Corps, July 9, 1942.
7. Theodorsen, Theodore, and Garrick, I. E.: Mechanism of Flutter—A Theoretical and Experimental Investigation of the Flutter Problem. NACA Rep. 685, 1940.
8. Timoshenko, S.: Vibration Problems in Engineering. D. Van Nostrand Co., Inc., 1928.
9. Diederich, Franklin W., and Budiansky, Bernard: Divergence of Swept Wings. NACA TN 1680, 1948.

TABLE I.—DATA FOR SHEARED

Model	$\Delta$ (deg)	$A_s$	$f_{h_1}$ (cps)	$f_{h_2}$ (cps)	$f_i$ (cps)	$f_a$ (cps)	$GJ$ (lb.-in. <sup>2</sup> )	$EI$ (lb.-in. <sup>2</sup> )	NACA airfoil section	$M_\infty$	$l$ (in.)	$c$ (in.)	$b$ (ft)	$x_{cg}$ (percent chord)	$x_{ac}$ (percent chord)	$x_{ac}'$ (percent chord)	$a+x_a$	$\alpha$	$r_{ac}$	$\frac{1}{\kappa}$	$\frac{p}{\rho}$ (slugs cu ft)	Percent Froon
Spruce wings																						
11A	0	2	45	272	108	107	15,000	25,100	16-005	0.89	16.0	8.0	0.333	48.4	45	45	-0.032	-0.10	0.333	13.3	0.00287	95
11A'	0	2	26	-----	59	37	-----	-----	16-005	0.89	16.0	8.0	0.333	48.4	26.6	26.6	-0.032	-0.468	0.395	17.6	0.0217	0
11B'	0	2	29	-----	61	43	-----	-----	16-005	0.89	16.0	8.0	0.333	48.4	29.7	29.7	-0.032	-0.406	0.371	40.5	0.00943	88
12	15	2	43	-----	103	108	14,400	54,700	16-005.2	0.88	16.6	7.72	0.321	48.5	45.3	46	-0.03	-0.074	0.33	5.69	0.00725	96
12	15	2	42	-----	105	106	14,400	54,700	16-005.2	0.88	16.6	7.72	0.321	48.5	45.3	46	-0.03	-0.074	0.33	5.47	0.00456	98
12	15	2	42	-----	103	102	14,400	54,700	16-005.2	0.88	16.6	7.72	0.321	48.5	45.3	46	-0.03	-0.074	0.33	11.2	0.00367	97
13	30	2	33	195	94	93	11,100	53,500	16-005.8	0.87	18.2	6.87	0.284	48.8	45.0	49	-0.024	-0.080	0.33	7.15	0.00746	99
14	45	2	22	139	93	92	9,240	33,000	16-007.1	0.85	22.6	5.52	0.234	48.8	45.0	60	-0.024	-0.080	0.33	7.78	0.00720	84
14	45	2	21	136	92	91	9,240	33,000	16-007.1	0.85	22.6	5.52	0.234	48.8	45.0	60	-0.024	-0.080	0.33	19.8	0.00285	94
16	60	2	19	68	93	92	4,520	19,100	16-010	0.81	32.0	4.0	0.167	48.8	45.0	65	-0.024	-0.080	0.33	9.10	0.00757	92
15	60	2	12	67	93	93	4,520	19,100	16-010	0.81	32.0	4.0	0.167	48.8	45.0	65	-0.024	-0.080	0.33	14.0	0.00493	90
Balsa wings																						
22'	15	2	31	155	63	61	-----	-----	16-005.2	0.88	16.6	7.72	0.321	48.8	42.4	42.4	-0.024	-0.152	0.292	2.19	0.00854	98
22'	15	2	31	154	64	62	-----	-----	16-005.2	0.88	16.6	7.72	0.321	48.8	42.4	42.4	-0.024	-0.152	0.292	3.32	0.00488	93
22'	15	2	31	154	64	62	-----	-----	16-005.2	0.88	16.6	7.72	0.321	48.8	42.4	42.4	-0.024	-0.152	0.292	18.7	0.0100	92
22	30	2	35	219	89	89	6,230	27,800	16-005.8	0.87	18.2	6.87	0.284	48.0	48.0	53	-0.04	-0.04	0.304	3.18	0.00824	99
23	30	2	34	216	89	89	6,230	27,800	16-005.8	0.87	18.2	6.87	0.284	48.0	48.0	53	-0.04	-0.04	0.304	8.54	0.00321	91
23	30	2	34	220	91	91	6,230	27,800	16-005.8	0.87	18.2	6.87	0.284	48.0	48.0	53	-0.04	-0.04	0.304	9.15	0.00300	99
23	30	2	34	216	89	89	6,230	27,800	16-005.8	0.87	18.2	6.87	0.284	48.0	48.0	53	-0.04	-0.04	0.304	14.9	0.00184	90
24	45	2	19	153	73	73	2,810	10,800	16-007.1	0.85	21.8	5.66	0.236	47.0	49.0	57	-0.06	-0.02	0.311	3.64	0.00784	85
24	45	2	19	152	73	75	2,810	10,800	16-007.1	0.85	21.8	5.66	0.236	47.0	49.0	57	-0.06	-0.02	0.311	8.40	0.00339	93
24	45	2	19	152	73	75	2,810	10,800	16-007.1	0.85	21.8	5.66	0.236	47.0	49.0	57	-0.06	-0.02	0.311	13.2	0.00216	91
24	45	2	19	152	73	74	2,810	10,800	16-007.1	0.85	21.8	5.66	0.236	47.0	49.0	57	-0.06	-0.02	0.311	29.4	0.00070	74
24	45	2	19	150	74	74	2,810	10,800	16-007.1	0.85	21.8	5.66	0.236	47.0	49.0	57	-0.06	-0.02	0.311	30.5	0.00063	89
25A	60	2	8.6	64	68	65	1,950	6,470	16-010	0.81	32.0	4.0	0.167	46.9	40.0	71	-0.062	-0.20	0.359	34.6	0.00054	88
25B	60	2	8.6	48	70	68	-----	8,500	16-010	0.81	32.0	4.0	0.167	46.9	40.0	71	-0.062	-0.20	0.359	9.36	0.00353	91

TABLE II.—ROTATED

Model	$\Delta$ (deg)	$A_s$	$f_{h_1}$ (cps)	$f_{h_2}$ (cps)	$f_i$ (cps)	$f_a$ (cps)	$GJ$ (lb.-in. <sup>2</sup> )	$EI$ (lb.-in. <sup>2</sup> )	NACA airfoil section	$M_\infty$	$l$ (in.)	$c$ (in.)	$b$ (ft)	$x_{cg}$ (percent chord)	$x_{ac}$ (percent chord)	$x_{ac}'$ (percent chord)	$a+x_a$	$\alpha$	$r_{ac}$	$\frac{1}{\kappa}$	$\left(\frac{p}{\rho}\right)$ (cu ft)	Percent Froon
Lengthwise laminations																						
30A	0	6.20	11.9	76.0	90.4	83.0	3,760	-----	16-010	0.81	24.8	4	0.167	46.0	35	35	-0.08	-0.30	0.311	36.8	0.00220	0
30B	0	6.20	12.0	72.6	90.0	88.0	3,760	6,920	16-010	0.81	24.8	4	0.167	46.0	40	40	-0.08	-0.20	0.277	37.8	0.00214	0
30B	30	4.65	12.1	73.0	91.0	88.8	3,760	6,920	16-010	0.81	24.8	4	0.167	46.0	40	40	-0.08	-0.20	0.277	37.7	0.00215	0
30B	30	4.65	12.0	73.0	90.0	88.0	3,760	6,920	16-010	0.81	24.8	4	0.167	46.0	40	40	-0.08	-0.20	0.277	37.8	0.00214	0
30B	45	3.10	12.1	73.0	91.0	88.8	3,760	6,920	16-010	0.81	24.8	4	0.167	46.0	40	40	-0.08	-0.20	0.277	37.8	0.00214	0
30B	45	3.10	12.2	73.0	90.0	88.0	3,760	6,920	16-010	0.81	24.8	4	0.167	46.0	40	40	-0.08	-0.20	0.277	37.8	0.00214	0
30B	60	1.55	12.0	72.5	90.0	88.0	3,760	6,920	16-010	0.81	24.8	4	0.167	46.0	40	40	-0.08	-0.20	0.277	39.8	0.00204	0
30C	0	6.20	12.2	69.0	86.0	75.8	4,000	6,950	16-010	0.81	24.8	4	0.167	48.5	39	39	-0.03	-0.22	0.292	40.5	0.00200	89
30C	0	6.20	12.2	69.0	86.0	75.8	4,000	6,950	16-010	0.81	24.8	4	0.167	48.5	39	39	-0.03	-0.22	0.292	98.9	0.000820	86
30C	0	6.20	12.3	70.0	84.0	74.2	4,000	6,950	16-010	0.81	24.8	4	0.167	48.5	39	39	-0.03	-0.22	0.292	92.6	0.00076	83
30C	15	5.78	12.2	69.0	86.0	75.8	4,000	6,950	16-010	0.81	24.8	4	0.167	48.5	39	39	-0.03	-0.22	0.292	92.0	0.00070	81
30C	30	4.65	12.2	69.0	86.0	75.8	4,000	6,950	16-010	0.81	24.8	4	0.167	48.5	39	39	-0.03	-0.22	0.292	40.0	0.00202	89
30C	30	4.65	12.2	70.0	88.5	76.2	4,000	9,950	16-010	0.81	24.8	4	0.167	48.5	39	39	-0.03	-0.22	0.292	81.4	0.00095	85
30C	30	4.65	12.2	70.0	88.5	76.2	4,000	9,950	16-010	0.81	24.8	4	0.167	48.5	39	39	-0.03	-0.22	0.292	80.0	0.00100	85
30C	45	3.10	12.2	70.0	87.5	76.2	4,000	6,950	16-010	0.81	24.8	4	0.167	48.5	39	39	-0.03	-0.22	0.292	45.2	0.00179	87
30D	15	5.78	13.2	80.2	87.1	82.4	4,350	-----	16-010	0.81	24.8	4	0.167	48	39.5	39.5	-0.04	-0.21	0.280	8.70	0.00933	99
30D	15	5.78	13.2	80.2	87.1	82.4	4,350	-----	16-010	0.81	24.8	4	0.167	48	39.5	39.5	-0.04	-0.21	0.280	8.72	0.00930	99
30D	15	5.78	13.3	80.2	87.1	82.4	4,350	-----	16-010	0.81	24.8	4	0.167	48	39.5	39.5	-0.04	-0.21	0.280	8.70	0.00927	99
30D	30	4.65	13.5	81.7	92.5	87.4	4,350	-----	16-010	0.81	24.8	4	0.167	48	39.5	39.5	-0.04	-0.21	0.280	8.90	0.00910	99
30D	45	3.10	13.5	81.7	88.2	83.4	4,350	-----	16-010	0.81	24.8	4	0.167	48	39.5	39.5	-0.04	-0.21	0.280	8.85	0.00905	99
30D	60	1.55	13.5	82.0	90.5	85.5	4,350	-----	16-010	0.81	24.8	4	0.167	48	39.5	39.5	-0.04	-0.21	0.280	9.54	0.00852	99
Chordwise laminations																						
40A	0	6.20	9.4	57.4	90.0	88.4	3,540	5,250	16-010	0.81	24.8	4	0.167	46	40	40	-0.08	-0.20	0.277	36.5	0.00222	0
40A	0	6.20	9.6	57.1	91.0	88.5	3,540	5,250	16-010	0.81	24.8	4	0.167	46	40	40	-0.08	-0.20	0.277	24.2	0.00334	90
40A	0	6.20	9.6	57.1	91.0	88.5	3,540	5,250	16-010	0.81	24.8	4	0.167	46	40	40	-0.08	-0.20	0.277	37.7	0.00215	89
40A	0	6.20	9.6	57.1	91.0	88.5	3,540	5,250	16-010	0.81	24.8	4	0.167	46	40	40	-0.08	-0.20	0.277	75.0	0.00108	82
40A	15	5.78	9.3	55.8	90.6	88.2	3,540	5,250	16-010	0.81	24.8	4	0.167	46	40	40	-0.08	-0.20	0.277	35.1	0.00231	0
40A	30	4.65	9.3	55.8	90.6	88.2	3,540	5,250	16-010	0.81	24.8	4	0.167	46	40	40	-0.08	-0.20	0.277	27.5	0.00316	0
40B	0	6.20	9.5	55.0	90.5	88.2	3,710	5,020	16-010	0.81	24.8	4	0.167	46	40	40	-0.08	-0.20	0.277	35.5	0.00228	0
40C	0	6.20	9.0	54.4	91.0	88.2	2,280	4,350	16-010	0.81	24.8	4	0.167	49	40	40	-0.02	-0.20	0.267	8.74	0.00628	100
40D	0	6.20	9.4	58.0	88.9	84.0	3,330	5,050	16-010	0.81	24.8	4	0.167	48	39.5	39.5	-0.08	-0.21	0.280	79.0	0.00969	84
40D	15	5.78	9.6	58.3	88.9	84.0	3,330	5,050	16-010	0.81	24.8	4	0.167	48	39.5	39.5	-0.04	-0.21	0.280	36.2	0.00212	89
40D	15	5.78	9.5	57.9	87.5	82.6	3,330	5,050	16-010	0.81	24.8	4	0.167	48	39.5	39.5	-0.04	-0.21	0.280	80.0	0.00956	87
40D	30	4.65	9.5	57.5	89.0	84.1	3,330	5,050	16-010	0.81	24.8	4	0.167	48	39.5	39.5	-0.04	-0.21	0.280	88.2	0.00967	85
40D	45	3.10	9.6	58.3	88.9	84.0	3,330	5,050	16-010	0.81	24.8	4	0.167	48	39.5	39.5	-0.04	-0.21	0.280	39.1	0.00196	86

## SWEEP MODELS—SERIES I

$f_e$ (cps)	$f_R$ (cps)	$f_A$ (cps)	$f_e$ $f_R$	$f_e$ $f_A$	$f_e$ $f_A$	$\phi$ (deg)	$\left(\frac{q}{b}\right)$ (lb/sq ft)	$M$	$V_e$ (mph)	$V_R$ (mph)	$V_R'$ (mph)	$V_A$ (mph)	$\frac{q}{b_{osc}}$	$\frac{V_e}{V_R}$	$\frac{V_e}{V_A}$	$V_D$ (mph)	Remarks
Spruce wings																	
66	70	-----	0.62	0.93	-----	50	235	0.82	274	260	260	-----	1.80	1.05	-----	214	Tunnel excitation frequency, 67 cps. Model failed. { Slotted 4 3/4 inches from trailing edge. Slots uncovered.
42	40	-----	1.12	1.03	-----	80	85.0	-.24	191	129	129	-----	3.68	1.48	-----	583	
38	42	-----	-.87	-.91	-----	170	70.5	-.74	262	197	197	-----	4.22	1.33	-----	183	
64	70	-----	-.63	-.92	-----	70	375	-.64	218	176	-----	1.64	1.24	-----	175		
62	71	71	-.87	-.87	0.87	50	320	-.71	345	206	-----	205	1.70	1.19	1.26	217	Tunnel excitation frequency, 61 cps.
55	69	69	-.54	-.80	-.80	50	307	-.79	276	225	-----	220	1.95	1.23	1.25	245	
61	60	65	1.01	-.94	-----	70	334	-.62	202	154	-----	159	1.77	1.31	1.27	149	
54	56	61	-.59	-.97	-.88	60	300	-.56	196	134	-----	166	2.11	1.45	1.18	119	
37	51	53	-.41	-.72	-.70	40	224	-.51	275	191	-----	245	2.99	1.44	1.12	187	
37	53	58	-.40	-.70	-.64	40	265	-.51	179	108	107	184	2.71	1.73	1.97	105	
36	51	55	-.39	-.71	-.65	30	264	-.62	222	124	127	222	3.35	1.79	1.00	122	
Balsa wings																	
50	46	---	0.82	1.07	---	70	101	0.30	104	97.3	---	---	1.25	1.07	---	79.9	Tunnel excitation frequency, 49 cps. Slotted 2 3/4 inches from trailing edge.
51	48	48	-.83	1.07	1.06	50	74.7	-.34	119	95.0	---	96	1.41	1.25	1.24	107	
45	46	46	-.72	-.96	-.98	50	54.2	-.42	224	167	---	168	2.64	1.34	1.33	238	
60	62	---	-.68	-.96	---	130	189	-.42	142	137	---	---	1.81	1.04	---	110	
62	62	65	-.70	1.01	-.95	70	162	-.62	212	176	---	175	1.95	1.21	1.21	150	Tunnel excitation frequency, 61 cps. Tunnel excitation frequency, 61 cps.
60	63	---	-.67	-.96	---	60	171	-.66	229	185	---	---	2.07	1.24	---	190	
53	60	65	-.59	-.87	-.82	90	152	-.81	275	221	---	224	2.53	1.24	1.23	237	
51	49	---	-.71	1.06	---	90	125	-.34	121	97.1	---	---	1.63	1.25	---	80.1	
49	49	58	-.65	1.00	-.84	40	120	-.54	190	132	---	145	2.35	1.37	1.24	127	
45	48	---	-.60	1.05	---	40	106	-.64	215	160	---	---	2.82	1.35	---	159	
---	44	---	---	---	---	---	83.5	-.76	261	226	---	---	3.78	1.25	---	232	
34	43	45	-.47	-.79	-.75	60	78.0	-.81	277	226	---	252	3.77	1.22	1.10	232	
29	37	40	-.44	-.75	-.72	10	76.8	-.79	272	161	189	278	5.90	1.69	1.98	210	Model failed. Model failed.
---	45	48	---	---	---	---	73.6	-.41	139	98.5	97.5	161	2.85	1.49	1.86	115	

## WINGS—SERIES II

$f_e$ (cps)	$f_R$ (cps)	$f_A$ (cps)	$\frac{f_e}{f_R}$	$\frac{f_e}{f_A}$	$\phi$ (deg)	$\left(\frac{q}{b}\right)$ (lb/sq ft)	$M$	$V_e$ (mph)	$V_R$ (mph)	$V_R'$ (mph)	$V_A$ (mph)	$\frac{q}{b_{osc}}$	$\frac{V_e}{V_R}$	$\frac{V_e}{V_A}$	$V_D$ (mph)	Remarks	
Lengthwise laminations																	
42	45	---	0.51	0.91	---	70	127	0.30	232	209	209	---	3.91	1.11	---	218	Wing failed; tunnel excitation frequency, 40.7 cps.
48	44	46	.54	1.08	1.04	60	121	.29	229	212	212	215	3.64	1.08	1.06	263	
51	47	47	.57	1.08	1.08	60	126	.30	235	214	214	229	3.74	1.10	1.03	266	
50	44	47	.57	1.14	1.08	40	129	.30	237	212	212	229	3.77	1.12	1.04	263	
---	44	47	---	---	---	---	166	.34	269	214	214	265	4.26	1.28	1.01	266	
55	44	47	.62	1.25	1.16	50	169	.35	272	212	212	265	4.32	1.28	1.02	263	Wing failed.
---	46	48	---	---	---	---	275	.45	350	219	219	353	5.59	1.60	1.99	265	
34	41	---	.45	.83	---	30	104	.63	219	159	159	---	4.05	1.16	---	249	
24	37	---	.32	.65	---	30	74.4	.81	286	260	260	---	5.29	1.86	---	393	
21	36	---	.29	.59	---	30	70.6	.82	268	270	270	---	5.43	1.07	---	369	
27	36	---	.36	.74	---	30	72.5	.78	278	262	262	---	5.18	1.95	---	376	
37	41	---	.48	.89	---	50	113	.65	226	187	187	---	4.18	1.21	---	245	
---	41	---	---	---	---	---	88.1	.81	284	263	263	---	5.22	1.06	---	355	
31	38	---	.40	.80	---	30	88.6	.81	268	260	260	---	5.32	1.11	---	352	
40	41	---	.33	.98	---	40	147	.76	273	199	199	---	5.02	1.37	---	265	
50	51	51	.61	.98	.98	50	110	.81	104	100	100	100	1.77	1.05	1.04	119	
51	52	52	.61	.98	.98	50	115	.82	107	100	100	101	1.82	1.08	1.06	119	
51	52	52	.61	.98	.98	50	121	.83	109	100	100	101	1.85	1.10	1.08	119	
53	54	56	.61	.98	.95	40	150	.88	123	106	106	116	1.97	1.16	1.08	129	
56	52	55	.67	1.08	1.02	60	178	.41	135	101	101	130	2.26	1.34	1.04	122	
65	63	67	.77	1.24	1.14	90	307	.65	182	107	107	182	2.98	1.70	1.00	130	
Chordwise laminations																	
62	47	---	0.70	1.33	---	140	82.0	0.24	188	211	211	---	2.98	0.892	---	260	Tunnel excitation frequency, 57 cps.
56	49	---	.63	1.15	---	60	86.7	.45	155	184	184	---	2.45	1.843	---	212	
61	46	---	.69	1.33	---	70	69.2	.50	172	215	215	---	2.72	1.800	---	265	
61	43	---	.69	1.44	---	70	63.6	.65	234	299	299	---	3.70	1.734	---	372	
61	46	---	.68	1.30	---	90	93.9	.26	201	308	308	---	3.19	1.967	---	254	
---	46	---	---	---	---	---	127	.30	235	213	213	---	2.73	1.10	---	263	Wing failed.
61	45	---	.71	1.37	---	10	77.7	.23	178	191	191	---	2.91	1.932	---	247	Wing failed.
29	36	---	.61	.83	---	80	57.6	.28	78.3	74.5	74.5	---	1.81	1.01	---	90.4	Wing failed.
62	40	---	.73	1.54	---	30	82.3	.62	221	261	261	---	3.69	1.787	---	270	Tunnel excitation frequency, 61 cps.
62	44	---	.74	1.41	---	70	72.7	.61	177	194	194	---	2.95	1.913	---	261	
61	40	---	.74	1.54	---	50	57.9	.67	236	279	279	---	3.99	1.845	---	267	
65	40	---	.77	1.63	---	60	79.4	.82	290	298	298	---	4.53	1.973	---	392	
32	44	---	.38	.73	---	90	138	.73	264	200	200	---	4.24	1.27	---	261	

## SWEEP FORWARD TESTS—SERIES III

$f_e$ (cps)	$f_R$ (cps)	$f_A$ (cps)	$f_e$ $f_R$	$f_e$ $f_A$	$f_e$ $f_A$	$\phi$ (deg)	$\frac{q}{b}$ (lb/sq ft)	$M$	$V_e$ (mph)	$V_R$ (mph)	$V_R'$ (mph)	$V_A$ (mph)	$\frac{q}{b_{osc}}$	$\frac{V_e}{V_R}$	$\frac{V_e}{V_A}$	$V_D$ (mph)	Remarks
---	98	---	---	---	---	---	73.4	0.26	88.9	174	174	---	0.888	0.498	---	294	Model diverged.
---	98	---	---	---	---	---	107	-.31	105	174	174	---	1.075	1.603	---	294	Model diverged.
102	79	---	0.77	1.29	---	40	211	-.40	303	219	219	---	3.18	1.649	---	579	Model failed.
61	94	---	-.73	-.97	---	100	260	-.62	170	172	172	---	2.05	1.989	---	704	
74	94	---	-.72	-.90	---	70	267	-.61	169	172	172	---	2.04	1.982	---	705	
84	93	---	-.63	-.80	---	160	352	-.61	202	179	179	---	2.44	1.125	---	720	
74	93	---	---	---	---	---	423	-.69	226	179	179	---	2.73	1.265	---	736	

TABLE IV.—SWEEPED MODELS OF A CONSTANT

Model	$\Lambda$ (deg)	$A_s$	$f_{h_1}$ (cps)	$f_{h_2}$ (cps)	$f_t$ (cps)	$f_a$ (cps)	$GJ$ (lb-in. <sup>2</sup> )	$EI$ (lb-in. <sup>2</sup> )	NACA airfoil section	$M_\infty$	$l$ (in.)	$c$ (in.)	$b$ (ft)	$x_{cg}$ (percent chord)	$x_{cm}$ (percent chord)	$x_{ca}$ (percent chord)	$a + x_a$	$\alpha$	$r_a^2$
62	15	7.95	4.9	29.1	72.5	71.8	3,730	7,820	16-010	0.81	34	4	0.167	41	44	46	-0.18	-0.12	0.175
62	15	7.95	4.9	29.1	73.4	72.5	3,730	7,820	16-010	.81	34	4	.167	41	44	46	-.18	-.12	.175
62	15	7.95	4.9	29.1	73.4	72.5	3,730	7,820	16-010	.81	34	4	.167	41	44	46	-.18	-.12	.175
62	15	7.95	4.9	29.6	73.5	72.7	3,730	7,820	16-010	.81	34	4	.167	41	44	46	-.18	-.12	.175
63	30	6.38	4.6	25.9	73.5	73.0	5,450	5,870	16-010	.81	34	4	.167	41	44	47	-.18	-.12	.175
63	30	6.38	3.9	24.0	73.0	73.4	5,450	5,870	16-010	.81	34	4	.167	41	44	47	-.18	-.12	.175
63	30	6.38	4.6	25.8	73.5	73.0	5,450	5,870	16-010	.81	34	4	.167	41	44	47	-.18	-.12	.175
63	30	6.38	4.0	24.0	73.0	72.4	5,450	5,870	16-010	.81	34	4	.167	41	44	47	-.18	-.12	.175
63	30	6.38	4.0	24.0	73.0	72.4	5,450	5,870	16-010	.81	34	4	.167	41	44	47	-.18	-.12	.175
63	30	6.38	4.0	24.0	73.0	72.4	5,450	5,870	16-010	.81	34	4	.167	41	44	47	-.18	-.12	.175
64	45	4.75	4.4	28.0	65.0	65.5	3,500	6,080	16-010	.81	34	4	.167	41	44	57	-.18	-.12	.175
64	45	4.75	4.2	27.0	65.0	65.5	3,500	6,080	16-010	.81	34	4	.167	41	44	57	-.18	-.12	.175
64	45	4.75	4.2	27.0	65.0	65.5	3,500	6,080	16-010	.81	34	4	.167	41	44	57	-.18	-.12	.175
64	45	4.75	4.1	27.0	65.0	64.4	3,500	6,080	16-010	.81	34	4	.167	41	44	57	-.18	-.12	.175
64	45	4.75	4.1	27.0	65.0	64.4	3,500	6,080	16-010	.81	34	4	.167	41	44	57	-.18	-.12	.175
65	60	2.12	5.7	33.4	77.0	76.2	4,650	11,980	16-010	.81	34	4	.167	41	44	71	-.18	-.12	.175

TABLE V.—DATA FOR SWEEPED MODELS OF A

Model	$\Lambda$ (deg)	$A_s$	$f_{h_1}$ (cps)	$f_{h_2}$ (cps)	$f_t$ (cps)	$f_a$ (cps)	$GJ$ (lb-in. <sup>2</sup> )	$EI$ (lb-in. <sup>2</sup> )	NACA airfoil section	$M_\infty$	$l$ (in.)	$c$ (in.)	$b$ (ft)	$x_{cg}$ (percent chord)	$x_{cm}$ (percent chord)	$x_{ca}$ (percent chord)	$a + x_a$	$\alpha$	$r_a^2$
72	15	6.09	7.6	54	97.3	96.3	3,730	7,820	16-010	0.81	26	4	0.167	41	44	46	-0.18	-0.12	0.175
72	15	6.09	7.6	54	97.3	96.3	3,730	7,820	16-010	.81	26	4	.167	41	44	46	-.18	-.12	.175
73	30	4.88	6.4	40.0	98.0	97.0	5,450	5,870	16-010	.81	26	4	.167	41	44	47	-.18	-.12	.175
73	30	4.88	6.4	40.0	98.0	97.0	5,450	5,870	16-010	.81	26	4	.167	41	44	47	-.18	-.12	.175
73	30	4.88	6.4	40.0	98.0	97.0	5,450	5,870	16-010	.81	26	4	.167	41	44	47	-.18	-.12	.175
74	45	3.25	6.5	40.0	79.0	77.2	3,500	6,080	16-010	.81	26	4	.167	41	44	57	-.18	-.12	.175
74	45	3.25	6.7	39.5	78.5	77.7	3,500	6,080	16-010	.81	26	4	.167	41	44	57	-.18	-.12	.175
74	45	3.25	6.7	39.5	78.5	77.7	3,500	6,080	16-010	.81	26	4	.167	41	44	57	-.18	-.12	.175
75	60	1.65	7.2	51.8	82.4	81.6	4,650	11,980	16-010	.81	26	4	.167	41	44	71	-.18	-.12	.175
75	60	1.65	7.2	51.8	82.4	81.6	4,650	11,980	16-010	.81	26	4	.167	41	44	71	-.18	-.12	.175

TABLE VI.—DATA FOR TIP-

Model	$\Lambda$ (deg)	$A_s$	$f_{h_1}$ (cps)	$f_{h_2}$ (cps)	$f_t$ (cps)	$f_a$ (cps)	$GJ$ (lb-in. <sup>2</sup> )	$EI$ (lb-in. <sup>2</sup> )	NACA airfoil section	$M_\infty$	$l$ (in.)	$c$ (in.)	$b$ (ft)	$x_{cg}$ (percent chord)	$x_{cm}$ (percent chord)	$x_{ca}$ (percent chord)	$a + x_a$	$\alpha$	$r_a^2$
84-1	45	3.63	10	60	133	104	-----	-----	16-010	0.81	29	4	0.167	51	32	44	0.02	-0.30	0.378
84-2	45	3.63	10	61	135	107	-----	-----	16-010	.81	29	4	.167	51	32	44	.02	-.36	.378
94-3	45	3.63	9.6	58	118	98	-----	-----	16-010	.81	29	4	.167	51.5	32	44	.03	-.36	.378
85-1	60	2.75	5.0	32	92	72	10,800	13,400	16-010	.81	44	4	.167	50	32	58	.0	-.36	.378
85-2	60	2.75	5.0	31	95	75	9,850	12,400	16-010	.81	44	4	.167	50	32	58	.0	-.36	.378
85-3	60	2.75	5.0	30	80	63	11,200	16,600	16-010	.81	44	4	.167	51	32	58	.02	-.36	.378

TABLE VII.—DATA FOR MODELS USED TO DETERMINE

Model	$\Lambda$ (deg)	$A_s$	$f_{h_1}$ (cps)	$f_{h_2}$ (cps)	$f_t$ (cps)	$f_a$ (cps)	$GJ$ (lb-in. <sup>2</sup> )	$EI$ (lb-in. <sup>2</sup> )	NACA airfoil section	$l$ (in.)	$c$ (in.)	$b$ (ft)	$x_{cg}$ (percent chord)	$x_{cm}$ (percent chord)	$x_{ca}$ (percent chord)	$a + x_a$	$\alpha$	$r_a^2$	$\frac{1}{\kappa}$
91-1	0	6	4.2	24	31	23	34,100	128,000	16-010	48	8	0.333	29.9	48	48	-0.402	-0.04	0.307	17.3
91-2	0	6	5.5	36	43	43	41,200	108,300	16-010	48	8	.333	41.0	43.8	43.8	-.18	-.124	.179	41.7
91-2	0	6	5.5	36	43	43	41,200	108,300	16-010	48	8	.333	41.0	43.8	43.8	-.18	-.124	.179	56.4
91-2	0	6	5.3	33	42	42	41,200	108,300	16-010	48	8	.333	41.0	43.8	43.8	-.18	-.124	.179	12.8
91-2	0	6	5.5	36	43	43	41,200	108,300	16-010	48	8	.333	41.0	43.8	43.8	-.18	-.124	.179	95.5
91-3	0	6	5.0	30	40	40	28,500	83,700	16-010	48	8	.333	49.0	48.4	48.4	-.02	-.032	.160	44.3
91-3	0	6	4.7	29	39	39	28,500	83,700	16-010	48	8	.333	49.0	48.4	48.4	-.02	-.032	.160	36.4
91-3	0	6	4.7	29	39	39	28,500	83,700	16-010	48	8	.333	49.0	48.4	48.4	-.02	-.032	.160	48.4
92-1	15	6.09	8.3	48	70	62	3,730	7,820	Modified	26	4	.167	31.2	44	46	-.376	-.12	.298	77.9
92-2	15	6.09	8.3	49	95	95	3,730	7,820	Modified	26	4	.167	42.9	44	46	-.142	-.12	.136	76.0
92-3	15	6.09	8.1	47	55	52	3,730	7,820	Modified	26	4	.167	54.5	44	46	.090	-.12	.411	74.5
93-1	30	4.42	6.3	40	78	68	5,450	5,870	Modified	23.6	4	.167	30	44	47	-.40	-.12	.310	78.0
93-2	30	4.42	6.3	44	99	99	5,450	5,870	Modified	23.6	4	.167	43	44	47	-.16	-.12	.134	74.0
93-3	30	4.42	6.3	51	54	50	5,450	5,870	Modified	23.6	4	.167	56	44	47	.12	-.12	.428	73.2
94-1	-(45)	3.81	4.5	26	38	35	2,120	4,520	Modified	30.5	4	.167	44.5	56	-----	-.11	.12	.427	68.2
94-2	-(45)	3.81	4.8	28	70	70	2,120	4,520	Modified	30.5	4	.167	57.0	56	-----	.14	.12	.134	68.2
94-3	-(45)	3.81	4.6	28	40	38	2,120	4,520	Modified	30.5	4	.167	69.3	56	-----	.386	.12	.307	68.2
95'-1	60	1.65	5.6	-----	54	50	1,900	4,560	Modified	26.4	4	.167	31.4	22	41	-.372	-.50	.267	75.8
95'-2	60	1.65	5.9	-----	71	47	1,900	4,560	Modified	26.4	4	.167	42.8	22	41	-.144	-.56	.308	73.0
95'-3	60	1.65	5.8	35	40	27	1,900	4,560	Modified	26.4	4	.167	54.3	22	41	.086	-.56	.779	69.0



## LENGTH-CHORD RATIO OF 8.5—SERIES IV

$\frac{1}{\kappa}$	$\left(\frac{\rho}{\text{slugs}}\right)$ (cu ft)	Percent Freon	$f_s$ (cps)	$f_R$ (cps)	$\frac{f_s}{f_R}$	$\frac{f_s}{f_R}$	$\varphi$ (deg)	$\left(\frac{q}{\text{lb}}\right)$ (sq ft)	$M$	$V_s$ (mph)	$V_R$ (mph)	$V_R'$ (mph)	$\frac{V_s}{V_R}$	$\frac{V_s}{V_R}$	$V_D$ (mph)	Remarks
13.5	0.00925	99	22	35	0.28	0.59	30	91.8	0.29	95.4	105	104	1.85	0.905	91.6	
37.5	0.0333	88	20	32	.28	.64	20	72.7	.41	143	187	171	2.78	.856	153	
59.5	0.0210	87	19	31	.26	.60	20	69.7	.49	175	206	---	3.37	.850	192	
130.0	0.00984	85	16	29	.22	.55	20	57.5	.68	234	300	---	4.50	.780	264	
15.2	0.0745	73	19	35	.27	.56	180	98.8	.29	111	111	---	2.12	1.000	97.6	
26.8	0.0424	98	18	33	.25	.56	110	78.0	.38	129	142	---	2.49	.908	128	
46.0	0.0246	50	22	32	.30	.69	180	82.1	.40	176	183	---	3.37	.902	170	
53.0	0.0214	94	19	31	.26	.61	140	74.0	.52	179	195	---	3.46	.918	180	
98.2	0.0116	92	15	29	.20	.50	120	62.2	.64	222	262	---	4.30	.845	245	
50.9	0.0217	0	19	28	.29	.67	30	69.6	.22	178	174	176	3.69	.995	186	
12.1	0.0914	97	---	32	---	---	---	70.6	.24	83.9	91	90	1.80	.923	81.3	No record.
41.9	0.0263	54	18	29	.27	.61	0	68.3	.36	155	160	160	3.21	.968	132	Record shown in figure 4.
51.3	0.0215	92	17	27	.26	.62	30	63.5	.47	165	172	171	3.59	.960	173	
116.0	0.00953	86	16	25	.26	.68	0	57.5	.66	235	248	---	5.10	.948	260	
44.1	0.0297	94	17	33	.22	.51	0	172	.67	284	186	---	4.29	1.258	176	

## CONSTANT LENGTH-CHORD RATIO OF 6.5—SERIES V

$\frac{1}{\kappa}$	$\left(\frac{\rho}{\text{slugs}}\right)$ (cu ft)	Percent Freon	$f_s$ (cps)	$f_R$ (cps)	$\frac{f_s}{f_R}$	$\frac{f_s}{f_R}$	$\varphi$ (deg)	$\left(\frac{q}{\text{lb}}\right)$ (sq ft)	$M$	$V_s$ (mph)	$V_R$ (mph)	$V_R'$ (mph)	$\frac{V_s}{V_R}$	$\frac{V_s}{V_R}$	$V_D$ (mph)	Remarks
37.2	0.00336	94	30	43	0.21	0.71	10	143	0.59	197	220	221	2.88	0.895	201	
81.5	0.0153	89	22	40	.22	.58	0	109	.74	255	318	319	3.78	.804	297	
34.7	0.0327	96	29	43	.30	.67	---	133	.57	193	216	214	2.78	.893	196	
57.4	0.0198	93	24	41	.24	.57	80	118	.69	234	273	---	3.38	.868	252	
108	0.0105	93	22	39	.22	.55	---	90.8	.82	280	363	---	4.05	.770	345	
14.2	0.0719	98	29	37	.37	.77	0	118	.35	118	115	---	2.11	1.025	111	Wing failed.
56.0	0.0197	93	26	38	.33	.77	0	104	.64	219	214	---	2.95	1.023	218	
120	0.00923	90	21	31	.28	.69	0	85.5	.53	291	308	---	5.24	.945	320	
15.8	0.0829	95	39	39	.47	.99	30	294	.64	181	127	128	3.11	1.425	113	Model damaged at root.
16.7	0.0783	100	39	38	.46	.97	0	295	.58	196	134	136	3.05	1.386	122	Rear half separated from base.

## EFFECT MODELS—SERIES VI

$\frac{1}{\kappa}$	$\left(\frac{\rho}{\text{slugs}}\right)$ (cu ft)	Percent Freon	$f_s$ (cps)	$f_R$ (cps)	$\frac{f_s}{f_R}$	$\frac{f_s}{f_R}$	$\varphi$ (deg)	$\left(\frac{q}{\text{lb}}\right)$ (sq ft)	$M$	$V_s$ (mph)	$V_R$ (mph)	$V_R'$ (mph)	$\frac{V_s}{V_R}$	$\frac{V_s}{V_R}$	$V_D$ (mph)	Remarks
9.15	0.00781	99	75	76	0.65	0.89	50	339	0.60	199	142	---	2.66	1.40	253	Tip perpendicular to air stream. Model failed.
9.25	0.00764	99	60	78	.51	.70	0	382	.63	213	146	---	2.80	1.47	269	Tip perpendicular to leading edge. Model failed.
9.55	0.00778	99	---	68	---	---	---	346	.60	201	127	---	3.02	1.58	229	Tip parallel to air stream. Model failed.
34.6	0.0206	0	35	43	.44	.72	---	225	.41	322	185	189	6.24	1.74	241	Tip perpendicular to air stream. Model failed.
34.1	0.0206	0	27	46	.33	.54	---	178	.35	278	189	186	5.21	1.47	348	Tip perpendicular to leading edge. Model failed.
34.5	0.0207	0	22	38	.32	.58	0	203	.39	304	159	159	6.77	1.91	295	Tip parallel to air stream. Model failed.

## EFFECT OF CENTER-OF-GRAVITY SHIFT—SERIES VII

$\left(\frac{\rho}{\text{slugs}}\right)$ (cu ft)	Percent Freon	$f_s$ (cps)	$f_R$ (cps)	$\frac{f_s}{f_R}$	$\frac{f_s}{f_R}$	$\varphi$ (deg)	$\left(\frac{q}{\text{lb}}\right)$ (sq ft)	$M$	$V_s$ (mph)	$V_R$ (mph)	$V_R'$ (mph)	$\frac{V_s}{V_R}$	$\frac{V_s}{V_R}$	$V_D$ (mph)	Remarks
0.0067	95	12.5	15	0.54	0.82	---	153	0.37	127	231	231	3.83	0.548	78.9	Model failed.
0.0239	0	16	19	.37	.81	---	40	.28	208	207	207	3.40	1.000	192	
0.0177	0	16	19	.38	.86	20	105	.32	239	239	239	3.93	1.000	224	
0.0783	81	20	21	.47	.94	40	128	.33	122	120	120	2.05	1.02	104	
0.0105	0	15	18	.35	.83	30	106	.40	308	308	308	4.97	.985	291	
0.0226	0	18	17	.45	1.09	100	61.5	.20	159	158	158	2.78	1.01	187	
0.0274	78	15	17	.39	.91	10	38.4	.39	142	141	141	2.54	1.01	139	
0.0207	75	14	16	.37	.89	0	57.2	.44	163	161	161	2.92	1.01	161	
0.0214	0	26	36	.42	.72	0	195	.38	293	415	422	6.60	.705	245	
0.0219	0	22	36	.23	.66	20	151	.33	265	258	257	3.76	.990	251	
0.0224	0	26	28	.49	.93	20	87.5	.25	191	176	177	5.12	1.09	237	
0.0199	0	26	26	.39	.65	---	225	.41	324	503	---	6.73	.645	267	
0.0210	0	23	37	.28	.64	70	156	.34	264	265	---	3.72	.997	257	
0.0212	0	23	27	.45	.85	20	77.2	.23	185	170	---	5.15	1.09	231	
0.0223	0	18	20	.51	.88	20	61.0	.20	160	160	---	6.38	1.00	122	
0.0223	0	18	23	.26	.78	---	62.2	.21	162	139	---	3.24	1.17	136	Section reversed.
0.0223	0	17	16	.44	1.04	40	39.5	.17	129	63.2	---	4.78	1.39	110	
0.0201	0	24	27	.49	.89	30	268	.44	345	279	300	5.20	1.24	∞	
0.0209	0	23	26	.48	.86	20	212	.40	307	186	189	9.15	1.66	∞	Slotted 2 1/8 inches from trailing edge.
0.0218	0	23	20	.84	1.03	30	125	.30	234	121	123	12.1	1.94	∞	